Icarus xxx (2014) xxx–xxx

Contents lists available at ScienceDirect

Icarus

journal homepage: www.elsevier.com/locate/icarus

Mixtures of clays and sulfates within deposits in western Melas Chasma, Mars

Catherine M. Weitz [a,*], Eldar Noe Dobrea [a], James J. Wray [b]

[a] Planetary Science Institute, 1700 E Fort Lowell, Suite 106, Tucson, AZ 85719, United States
[b] School of Earth and Atmospheric Sciences, Georgia Institute of Technology, Atlanta, GA 30332, United States

ARTICLE INFO

Article history:
Received 19 December 2013
Revised 27 March 2014
Accepted 14 April 2014
Available online xxxx

Keywords:
Mars, surface
Geological processes
Spectroscopy
Mineralogy

ABSTRACT

We have utilized several data sets from multiple spacecraft that have been acquired over a continuous observation campaign across the southwestern Melas Chasma region of Mars. The blocky deposit observed on the chasma floor and on portions of the southern wallrock consists of mixtures of light- and medium-toned materials that exhibit displacement structures consistent with transport down the wallrock and onto the chasma floor. CRISM visible and near-infrared reflectance spectra of the light-toned blocks suggest mixtures of nontronite, jarosite, Al-clays, hydrated silica, and/or an acid leached clay. The medium-toned blocks typically lack spectral features or exhibit signatures of polyhydrated sulfates. Bright layered mounds embayed by blocky deposit materials display spectra consistent with Ca-sulfates (gypsum and/or bassanite) that may have resulted from precipitation of less soluble Ca-rich minerals during ponding and evaporation of dilute fluids along the western chasma floor.

Draping across some wallrock slopes is a light-toned deposit that sometimes overlies a blocky, layered, and spectrally bland medium-toned deposit. The light-toned deposit exhibits spectra consistent with mixtures of materials that may include jarosite, acid-leached clays, silica, poorly crystalline clays, and polyhydrated sulfates. Hesperian-age valleys dissect the medium-toned deposit along some wallrock slopes and may be partially filled in by light-toned deposits. The draping nature of these deposits can best be explained by airfall, either volcanic ash or atmospheric dust, with ice/snow accumulation perhaps controlling sedimentation along the wallrock. An examination of other regional hydrated deposits around southwestern Melas indicates similar draping deposits occur farther east and west along the wallrock, whereas layered sulfates to the southeast consist of monohydrated and polyhydrated sulfates that are similar to interior layered deposits found in many of the chasmata. Small opal and jarosite exposures within the Melas basin and along the nearby plateau are most likely the result of younger localized alteration and deposition. The diversity of hydrated minerals and fluvial features indicates multiple episodes of aqueous activity under distinct environmental conditions occurred throughout southwestern Melas Chasma during the Hesperian to Amazonian that may be contemporaneous with late aqueous activity elsewhere on Mars.

1. Introduction

Valles Marineris contains some of the largest exposures of light-toned sedimentary deposits on Mars. Many of these deposits, commonly referred to as interior layered deposits (ILDs), contain hydrated minerals (e.g. Gendrin et al., 2005; Murchie et al., 2009c; Roach et al., 2010; Weitz et al., 2012), indicating the role of water in their formation and possibly deposition. There are many hypotheses for the formation of the ILDs in Valles Marineris, including: (1) lacustrine sedimentary deposits (McCauley, 1978; Nedell et al., 1987; Komatsu et al., 1993; Malin and Edgett, 2000, 2001), (2) volcanic deposits (Peterson, 1982; Lucchitta, 1990; Lucchitta et al., 1994; Chapman and Tanaka, 2001; Hynek et al., 2003); (3) mass wasted material from the walls (Nedell et al., 1987; Lucchitta et al., 1994); and (4) eolian/airfall deposits (Peterson, 1982; Nedell et al., 1987; Malin and Edgett, 2000; Catling et al., 2006). More recent hypotheses include spring mounds (Rossi et al., 2008), trapping dust and sulfur aerosols within ice deposits (Niles and Michalski, 2009; Michalski and Niles, 2012), and cementation of eolian material during groundwater upwelling events (Andrews-Hanna et al., 2010; Murchie et al., 2009c).

* Corresponding author.
E-mail address: weitz@psi.edu (C.M. Weitz).

http://dx.doi.org/10.1016/j.icarus.2014.04.009
0019-1035/

The formation of Valles Marineris likely began in the Early Hesperian (Scott and Tanaka, 1986), with rifting associated with the Ius–Melas–Coprates graben thought to have occurred primarily during the Amazonian (Schultz, 1998). Along the boundary between western Melas Chasma and eastern Ius Chasma (Fig. 1), a deposit composed of rounded blocks (hereby referred to as "blocky deposit") is observed on the chasma floor. Weitz et al. (2003) analyzed the Melas blocky deposit using older Mars Observer Camera (MOC) images as a potential landing site for the Mars Exploration Rovers. They proposed a subaqueous landslide or a water-bearing source material to explain their observations, including evidence for blocks appearing to push into each other and fold structures within the blocks. Two additional but smaller blocky deposits occur farther north along the Melas Chasma floor (Weitz et al., 2003). Images of the blocky deposit towards the northeast (BD_3 in Weitz et al., 2003) indicate it is heavily mantled by eolian material and adjoined to an ILD within Melas Chasma. The smaller blocky deposit adjacent to the northern Melas wallrock (BD_2 in Weitz et al., 2003) appears to contain monohydrated and polyhydrated sulfates (Chojnacki and Hynek, 2008). Because our focus is on southwestern Melas Chasma, we do not discuss these northern blocky deposits in this paper.

A more recent study of the blocky deposit by Metz et al. (2010) defined the blocks as detached slabs consistent with isolated rounded blocks of material with localized evidence for stratification. They suggested the Melas blocky deposit and several others found throughout Valles Marineris resulted from slow subaerial or subaqueous landsliding and liquefaction. Because the blocky deposit is spatially separated, appears morphologically distinct, and is much thinner than the ILD mounds, its relationship to the ILDs remains uncertain.

In addition to the blocky deposit, southwestern Melas chasma also contains the Melas basin, an elevated 30×120 km enclosed basin with a postulated paleolake and aqueous landforms (Mangold et al., 2004; Quantin et al., 2005). The site was proposed as a candidate landing site for the Mars Science Laboratory (MSL) rover (Grant et al., 2011) due to the strong evidence for lacustrine deposits and fans, including deltas (Metz et al., 2010). The Melas basin has been studied in detail (e.g., Quantin et al., 2005; Williams and Weitz, 2014), but its relationship to the Melas blocky deposit and nearby wallrock deposits have not yet been analyzed. Given the scientific interest of the southwestern Melas chasma region and its potential for a future Mars rover landing site, a detailed investigation of this region, particularly to understand the role of aqueous activity, seems warranted at this time.

Thanks to the long-term acquisition of data through extensive targeting across the southwestern Melas region by the Mars Reconnaissance Orbiter (MRO) spacecraft, there is a wealth of information concerning the geology and mineralogy of this intriguing area. In this paper, we utilize several data sets from multiple spacecraft to understand the mineralogy, morphology, and stratigraphy of the Melas blocky deposit in order to further investigate its origin. In addition, we explore the regional geology of southwestern Melas Chasma to place the blocky deposit in geologic context and understand its possible relationship to other aqueous deposits and features in this region.

2. Data sets

We employed numerous martian data sets representing a range of spatial and spectral resolution, including the Mars Global Surveyor Mars Orbiter Laser Altimeter (MOLA, Zuber et al., 1992), Mars Odyssey Thermal Emission Imaging System (THEMIS, Christensen et al., 2004), Mars Express High Resolution Stereo Camera (HRSC, Jaumann et al., 2007), Mars Reconnaissance Orbiter (MRO) High Resolution Imaging Science Experiment (HiRISE, McEwen et al., 2007), MRO Compact Reconnaissance Imaging Spectrometer for Mars (CRISM, Murchie et al., 2007), and MRO Context Imager (CTX, Malin et al., 2007).

Regions of interest were initially identified from earlier Mars Observer Camera (MOC) images, and then targeted for MRO images. As MRO images were analyzed, we identified additional areas where geologic contacts and stratigraphy appeared to provide key relationships to decipher the sequence of events that emplaced the deposits. CRISM images were used to understand the composition and distribution of hydrated minerals within this region, and subsequently to identify other areas to target with additional HiRISE and CRISM images. Single HiRISE images that appeared to show important stratigraphic relationships and

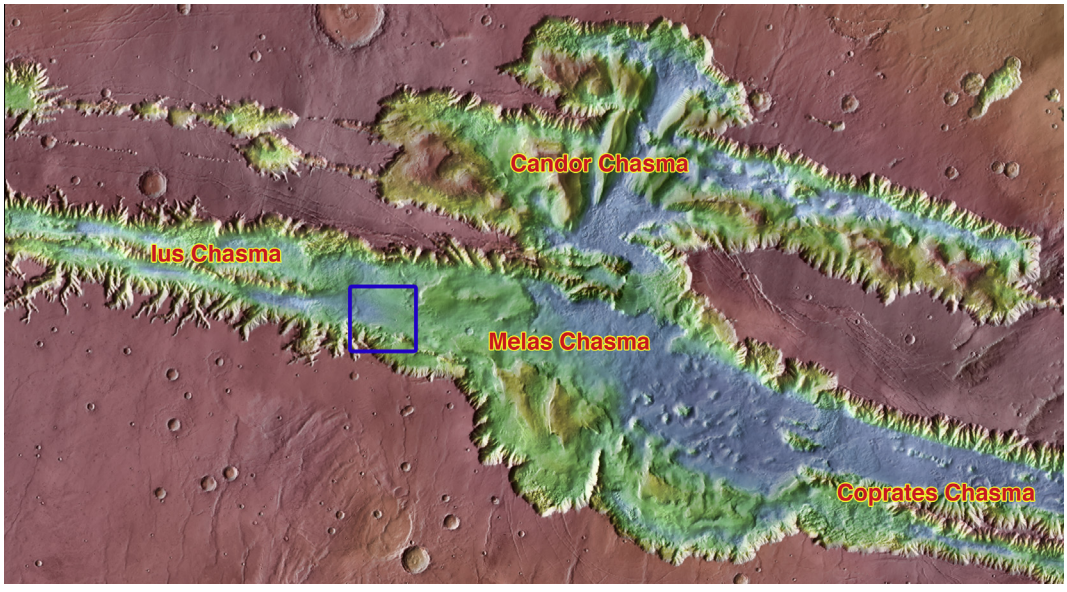

Fig. 1. MOLA topography displayed in color, where red represents approximately + 4000 m above and blue represents −5000 m below the martian datum, overlain on THEMIS daytime IR mosaic of central Valles Marineris. Blue box indicates location of study region in western Melas Chasma (Fig. 2). (For interpretation of the references to color in this figure legend, the reader is referred to the web version of this article.)

Please cite this article in press as: Weitz, C.M., et al. Mixtures of clays and sulfates within deposits in western Melas Chasma, Mars. Icarus (2014), http://dx.doi.org/10.1016/j.icarus.2014.04.009

topography were requested for stereo pairs. The targeting and acquisition of multiple images from several different MRO instruments occurred over several years using this iterative process of identifying key regions for additional observations based upon initial imaging analyses. Hence, the necessity and utility of long term observations by MRO facilitated this research and allowed us to complete a detailed and comprehensive evaluation of this scientifically exciting and complex region.

CRISM collects ~10-km-wide images from 0.4 to 3.9 μm with a pixel scale of 18 m/pixel in the full resolution targeted (FRT) mode and at ~40 m/pixel in the half-resolution short or long (HRS/HRL) mode (Murchie et al., 2009a). Typical data processing steps in CRISM analyses involve radiometric corrections (e.g., correction for the solar irradiance and geometry), photometric correction (correction for lighting and viewing geometry), atmospheric correction, and band parameterization and mapping (Murchie et al., 2009a). Radiometric correction is performed using a pipeline procedure that has been developed for the instrument. Atmospheric correction is performed using a scaled atmospheric template derived from observations of Olympus Mons (Murchie et al., 2009a). Finally, spectral parameter maps corresponding to diagnostic mineralogies are generated. The parameterizations employed herein are the same as those currently being used by the CRISM team to map the distribution of minerals such as clays, sulfates, pyroxenes, and olivines (Pelkey et al., 2007; Murchie et al., 2009b). In order to correlate mineralogy to morphology, these CRISM spectral parameter color maps were registered to HiRISE images.

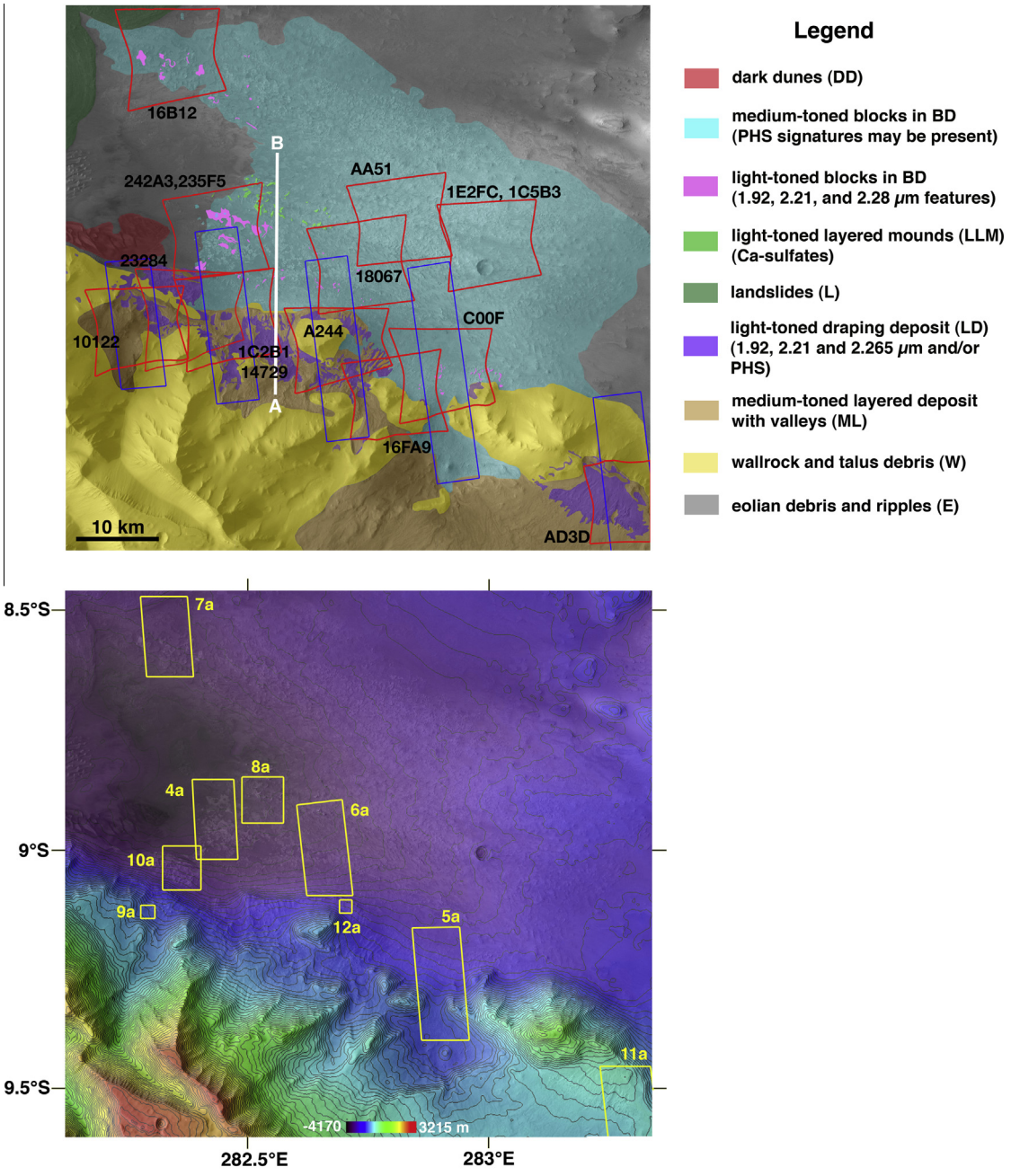

Fig. 2. (a) Geologic map of the units in our Melas study region. Red outlines and labels indicate CRISM images analyzed in this study, while blue rectangles are locations of HiRISE DTMs produced for this study. (b) HRSC-derived topography overlain on a portion of HRSC image H5178_0000. Contour intervals are at 100 m spacing. Yellow boxes indicate locations of later figures. (For interpretation of the references to color in this figure legend, the reader is referred to the web version of this article.)

Please cite this article in press as: Weitz, C.M., et al. Mixtures of clays and sulfates within deposits in western Melas Chasma, Mars. Icarus (2014), http://dx.doi.org/10.1016/j.icarus.2014.04.009

CRISM TRR3 images (calibration level 3) include a robust flat field correction, a correction for the effects of unremoved water vapor in observations of the ground calibration source to which inflight radiometric calibration is traced, and corrections for the effects of slight observation-to-observation irreproducibility in the viewing geometry of the inflight calibration reference (Seelos, 2011). All CRISM TRR3 images within our study area were examined. Corrected *I*/*F* spectra were extracted from regions of interest (typically greater than 5 × 5 pixels in area) and then each spectrum of interest was divided by a denominator spectrum of a spectrally unremarkable region extracted from the same column(s) as the spectrum of interest to account for column-dependent systematic errors (Murchie et al., 2007, 2009a). These ratioed spectra, plotted as relative *I*/*F* values, were then compared to laboratory data of pure minerals for potential matches. Difficulties associated with finding a perfect match to laboratory spectra can sometimes be attributed to subpixel mixing in the CRISM data, so in some cases plausible mineral mixtures are suggested on the basis of the positions of absorption bands in the spectrum.

A critical element of this study is to understand the morphological, mineralogical, and stratigraphic context of the blocky deposit. To accomplish this, we have co-registered available imagery from the CTX and HiRISE cameras to a THEMIS daytime IR mosaic basemap. HiRISE (~25 cm/pixel spatial scale) and CTX (~6 m/pixel) images, including stereo pairs, of the blocky deposit and geologic contacts with adjacent units have allowed us to determine stratigraphic relationships. Color HiRISE products were also utilized and include enhanced RGB and IRB images (McEwen et al., 2007).

Digital Terrain Models (DTMs) were generated using the commercial SOCET Set image analysis software for select locations where HiRISE stereo coverage exists (Fig. 2a). These HiRISE DTMs have elevation postings every 0.2 m (Kirk et al., 2008) and were analyzed to establish stratigraphic relationships, especially where distinct minerals were identified. In addition, they were used for determining absolute values in elevation, unit thicknesses, and to compute surface slopes. CRISM spectral parameter maps were co-registered and overlain on each DTM to aide in the interpretation of stratigraphic relationships of different hydrated units. A HRSC DTM (Jaumann et al., 2007) at 75 m/pixel resolution that covered the entire study area was utilized as well (H5178_0000).

We define and map units based upon morphology, which includes brightness. The terms "light-, medium-, and dark-toned" as used herein do not refer to a specific albedo range but rather to a unit's reflectance relative to other units within the same HiRISE image. The relative brightness between images can vary because different stretches were applied to each image. All images are shown with north at the top unless noted otherwise.

3. Geologic units

In this section, we analyze HiRISE, CTX, and HRSC images to determine physical properties and morphologies of the various deposits. From these observations, we mapped out the different geologic units shown in Fig. 2 and discussed below.

3.1. Blocky deposit (BD)

Much of the floor of Melas chasma in our study region consists of the blocky deposit, BD (Fig. 2a). Using HRSC-derived topography, unit BD can be traced upwards to the −1600 m contour along the wallrock, indicating that portions of the deposit occur along the wallrock slopes. The lowest elevation is at −4150 m on the western edge of the chasma floor. Unit BD generally consists of mixtures of light- and medium-toned blocks within a medium-toned matrix, where we define blocks as individual slabs with traceable edges whereas the matrix lacks slabs. Interspersed between and sometimes on the blocks is dark-toned eolian debris and ripples. The medium-toned blocks have rounded outlines and edges, and range from tens of meters to about 1 km in diameter. The interiors of medium-toned blocks contain either homogeneous exposures of heavily fractured rocks at the meter scale (Fig. 3b) or heterogeneous mixtures of light-and medium-toned materials (Fig. 3c).

The shape of the light-toned blocks (Fig. 4) generally appears more irregular with only the smaller blocks (tens of meters) displaying oval shapes. Materials within these light-toned blocks may exhibit banding, faults, and rugged high-standing exposures, as well as mixtures of different light- and medium-toned rocks (Fig. 4d and e). Stereo HiRISE images viewed as anaglyphs (Fig. 4c) show several medium-toned blocks stratigraphically above the light-toned blocks, indicating they are younger or were displaced above the light-toned blocks. Because the medium- and light-toned blocks are different in morphology and, as we will show in a later section, appear distinct spectrally, we distinguish and map them as individual materials within BD.

Evidence for deformation features within BD is shown in Fig. 5. Dark-toned materials appear to have slid down the wallrock slopes and now embay older medium-toned blocks. Folds can be seen in one of the blocks and have been displaced around a medium-toned block (Fig. 5b). Fig. 5 also shows smaller outcrops of older light-toned rocks that have been embayed and partially buried beneath the medium-toned blocks. These light-toned outcrops are now

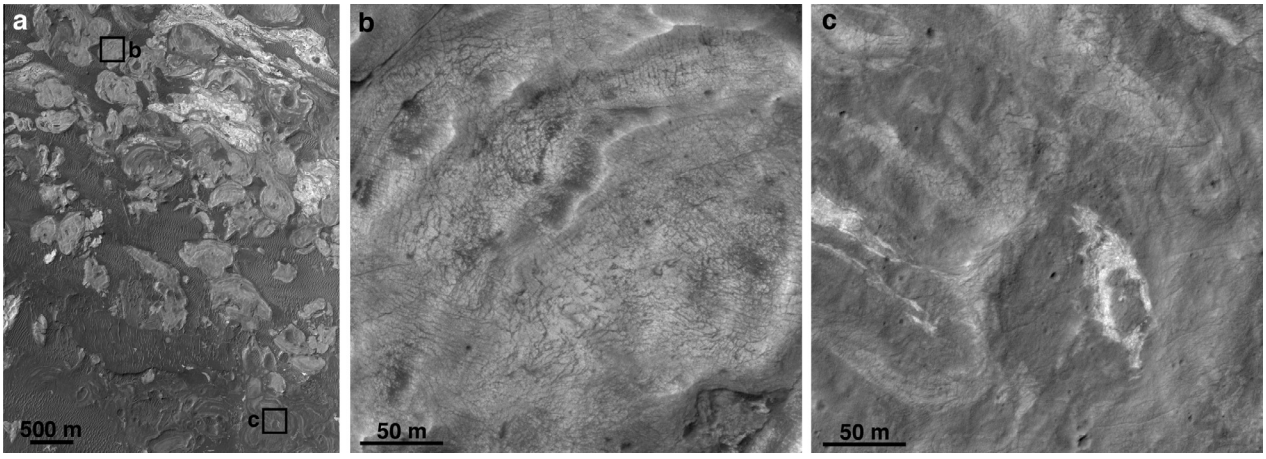

Fig. 3. (a) Examples of medium-toned blocks within the blocky deposit. Portion of HiRISE image ESP_026655_1710. (b) Homogeneous, heavily fractured block and (c) heterogeneous mixture of different materials within a block.

Please cite this article in press as: Weitz, C.M., et al. Mixtures of clays and sulfates within deposits in western Melas Chasma, Mars. Icarus (2014), http://dx.doi.org/10.1016/j.icarus.2014.04.009

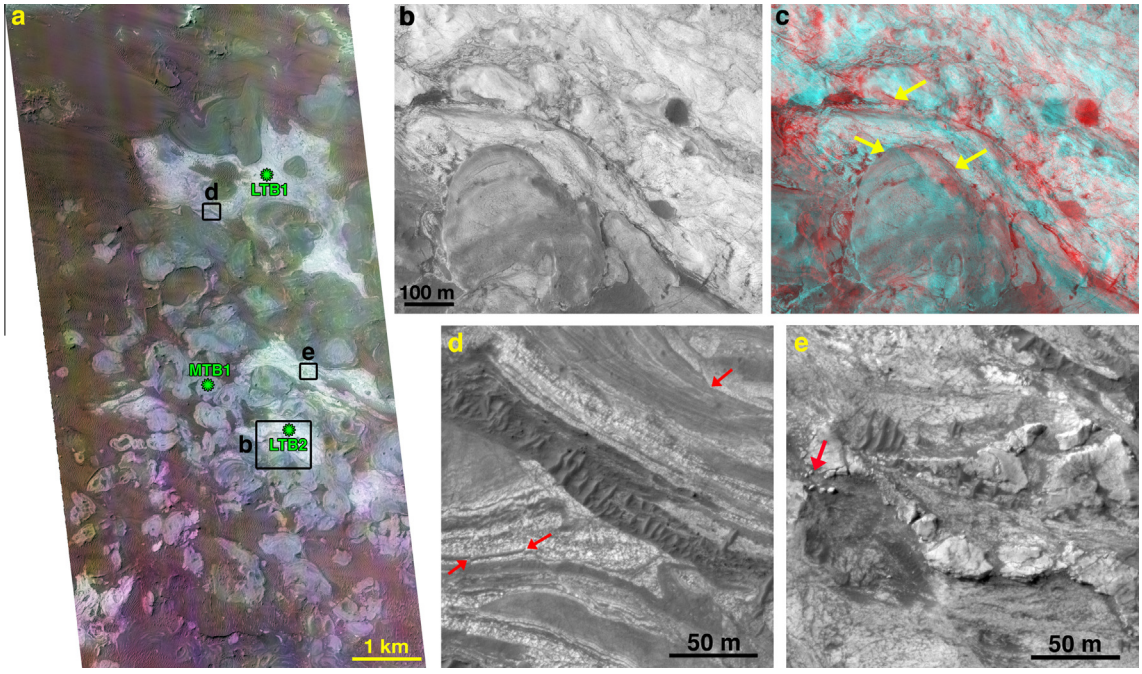

Fig. 4. Examples of materials within the blocky deposit. (a) Portion of HiRISE image ESP_026655_1710 overlain with CRISM FRT235F5 spectral parameter colors (red = olivine index that corresponds to olivine and Fe-containing phyllosilicates, green = band depth at 1.9 μm that corresponds to bound H_2O, blue = doublet absorption between 2.2 and 2.3 μm) (Murchie et al., 2009b). Rectangles identify blowup locations while asterisks show where CRISM spectra were extracted and labels correspond to those plotted in Fig. 13a. (b) Contact between light- and medium-toned materials within the blocky deposit. (c) Stereo anaglyph showing the same region in (b). Yellow arrows identify where the medium-toned materials overlie light-toned materials. (d) Example of layering and faulting (red arrows) within the light-toned blocks. Note that both light-toned and medium-toned materials are mixed together within these blocks. Dark-toned eolian ripples can also be seen covering portions of the blocky materials. (e) High-standing boulder-forming outcrops (red arrow) within the light-toned blocks. (For interpretation of the references to color in this figure legend, the reader is referred to the web version of this article.)

only visible as mounds and peaks within BD, typically <10 m in height (Fig. 5e).

Along a ~6° slope within unit BD, we have identified another example of folds and evidence for flow within the blocky deposit materials (Fig. 6). The folds have no topography associated with them as viewed in a HiRISE DTM (Fig. 6b) and, therefore, they are not exposures of layered sediments eroding around a topographic mound to give the appearance of folds. The folds indicate a downslope trend from southeast to northwest, which is also consistent with a SE–NW axial trace preference noted by Metz et al. (2010). The folds are alternating light- and medium-toned layers that experienced both ductile and brittle deformation (Fig. 6c).

Blocks in the northwestern portion of BD are shown in Fig. 7. These blocks display the greatest relief as viewed in a stereo anaglyph (Fig. 7b), either because they lack matrix material filling in the adjoining spaces between the blocks and/or there has been greater erosion here relative to the rest of unit BD. Surrounding many of the blocks are mesas covered by eolian ripples. Because the western portion of BD lies at lower elevations relative to the eastern side (Fig. 2b), eolian debris would be more likely to accumulate here. Situated adjacent to BD is a ~130-m high landslide deposit, whose edge can be seen in Fig. 7a and b, that originated from the northern wall of Melas Chama. Unfortunately, eolian material obscures the geologic contact between the two units, precluding a relative age determination.

Meter-scale layering is visible in some of the blocks and matrix material of BD, particularly along the northernmost region. The bedding appears to be a few meters thick and dozens of beds are apparent within some exposures. At HiRISE scales, the bedding appears similar in morphology and color throughout the exposed strata (Fig. 7d). In the few examples where bedding can be identified within individual blocks, it is most prominent near the center of the block but cannot always be traced towards the block edges.

3.2. Light-toned layered mounds (LLM)

Near the center of unit BD, we observe very bright and irregularly shaped mounds that appear distinct in morphology from other blocks in BD (Figs. 6f and 8). Vertical exposures across these mounds reveal a dozen or so meter-thick beds. The surfaces appear smoother with less fracturing than those observed in the light-toned blocks noted previously. Nevertheless, fracturing and erosion of these materials has produced meter-size blocks and talus seen adjacent to the outcrops (Fig. 8d). HiRISE stereo images show some outcrops with steep escarpments (Fig. 8b) and HRSC DTM-derived heights indicate some mounds are over 100 m high. Based upon superposition relationships interpreted from stereo HiRISE images (Fig. 8b), LLM appears to represent older rocks that have been embayed by BD materials.

3.3. Light-toned draping deposit (LD)

Our study region includes the wallrock that defines the southwestern edge of Melas Chasma (Fig. 2). The wallrock exhibits 'spur and gully' morphology or smooth talus slopes, with layering apparent along higher elevations where it has not been obscured beneath talus. We map a light-toned deposit draping across some wallrock slopes as unit LD. Analysis of the HRSC DTM (Fig. 2b) indicates the light-toned deposits reach as high as −640 m in elevation and can drape along slopes as steep as 18°. In HIRISE images, LD appears to be a thin (<5 m) patchy unit with extensive meter-scale fracturing (Figs. 9 and 10). Unit LD does not appear along the steepest wallrock slopes (~26°) but rather is confined to shallower slopes (Fig. 9c). It displays some layering with each layer appearing distinct in brightness (Figs. 9d and 10c). Portions of LD are covered by eolian ripples and darker mass wasting debris shedding from wallrock slopes. It is likely that LD was once more extensive across

Please cite this article in press as: Weitz, C.M., et al. Mixtures of clays and sulfates within deposits in western Melas Chasma, Mars. Icarus (2014), http://dx.doi.org/10.1016/j.icarus.2014.04.009

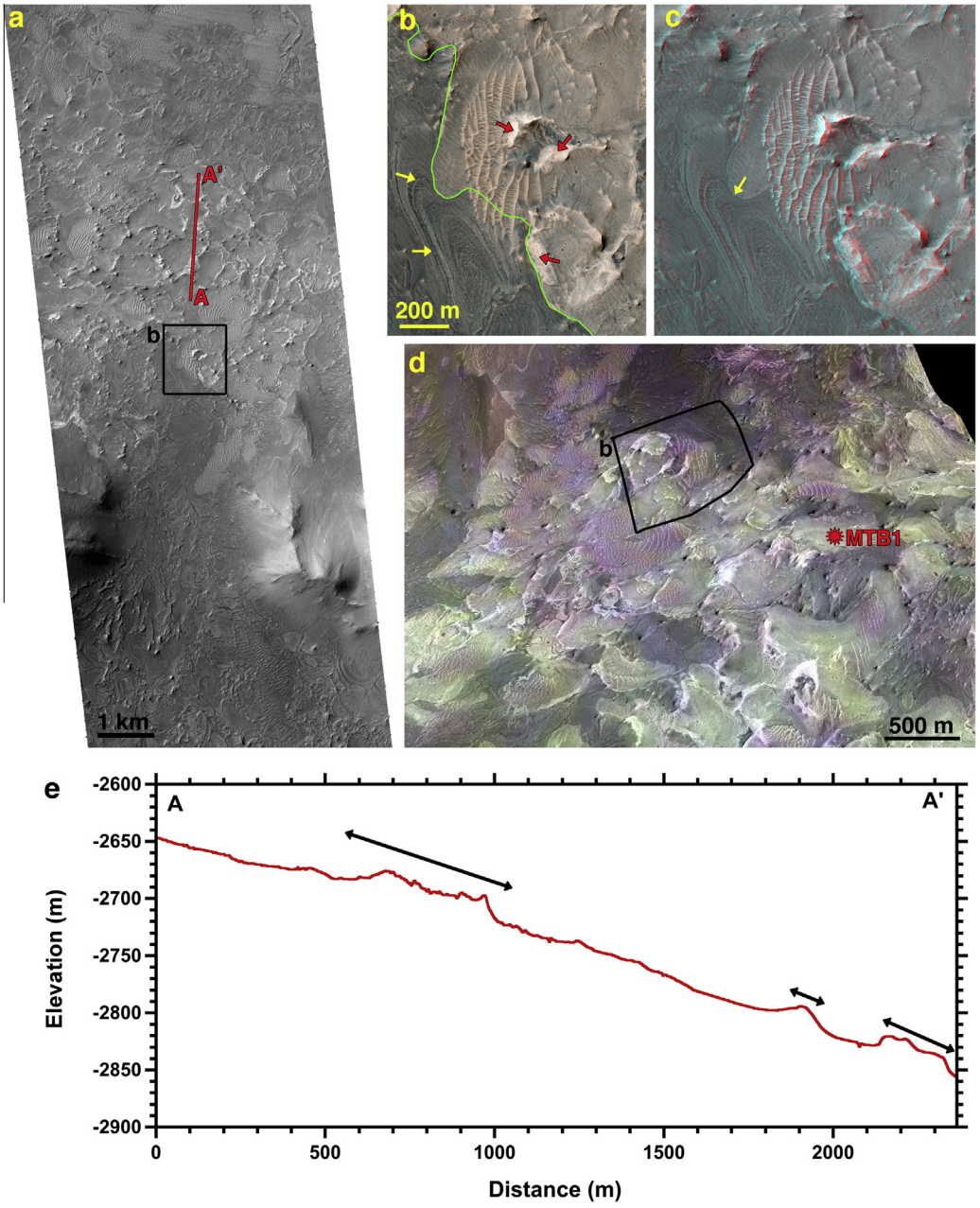

Fig. 5. (a) Portion of HiRISE image ESP_009592_1705 indicating location of blowup and topographic profile shown in e. (b) HiRISE enhanced color image showing boundary (green line) between dark- and medium-toned materials within BD. Yellow arrows note where folds can be seen while red arrows identify light-toned outcrops. (c) HiRISE stereo anaglyph of the same area shown in (b) with yellow arrow indicating where layers in the dark-toned material have been forced to flow around medium-toned materials. (d) HiRISE DTM perspective view at 10× vertical exaggeration looking southward (upslope). CRISM spectral parameters from FRTC00F are overlain in color on the DTM, where red is olivine index, green is band depth at 1.9 μm, and blue is band depth at 2.5 μm. Red asterisk and label corresponds to location where CRISM spectrum MTB1 was taken (see Fig. 13a). The light-toned outcrops correspond to high-standing mounds of older rocks that have been embayed by the medium-toned materials. (e) HiRISE-derived topographic profile showing the high-standing light-toned mounds (black lines with arrows) are typically <10 m in height. (For interpretation of the references to color in this figure legend, the reader is referred to the web version of this article.)

the wallrock slopes, but is now only preserved in areas where eolian erosion and mass wasting has not removed or covered it. Erosion of LD explains its general patchy appearance and has produced unusual branching ridges and rounded mounds (Fig. 9e) that do not exhibit any preferred orientation.

3.4. Medium-toned layered deposit (ML)

Covering much of the wallrock in our study region (Fig. 2) and sometimes underlying unit LD is a medium-toned deposit that appears blocky at the meter-scale and generally exhibits layering, which we map as unit ML. Layering can either be homogeneous with no tonal differences between all layers, or mixtures of brighter and darker layers. From HiRISE stereo images, we observe that ML drapes wallrock exposures (Figs. 9 and 10). The thickness of ML varies from a few to perhaps 20 m. Valleys dissect portions of ML, although in this region the valleys are not as dense or organized as those mapped farther east that drain into a postulated paleolake and are thought to have formed in the Late Hesperian by atmospheric precipitation (Mangold et al., 2004; Quantin

Please cite this article in press as: Weitz, C.M., et al. Mixtures of clays and sulfates within deposits in western Melas Chasma, Mars. Icarus (2014), http://dx.doi.org/10.1016/j.icarus.2014.04.009

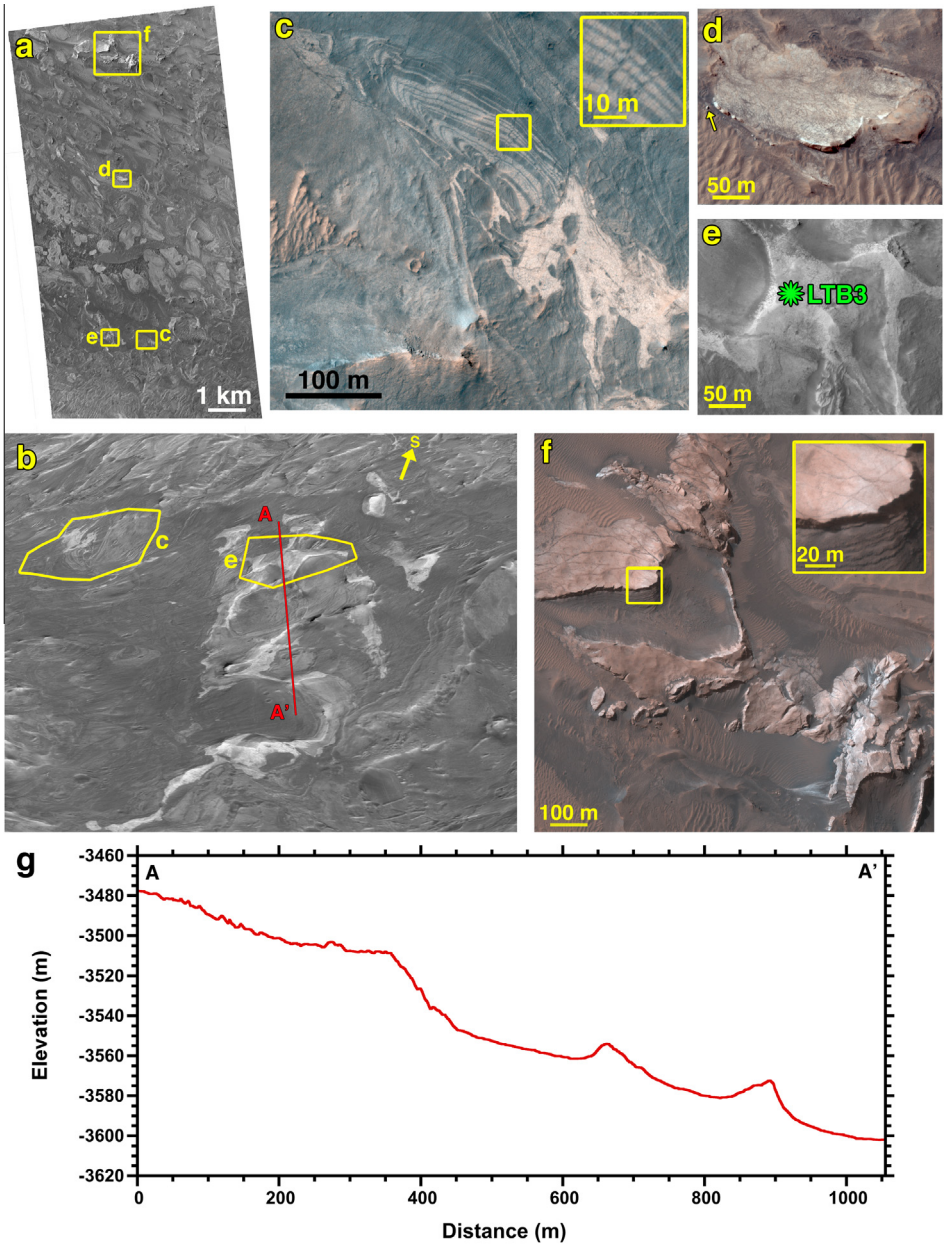

Fig. 6. (a) Portion of HiRISE image PSP_007443_1705 showing numerous blocks within unit BD. Yellow rectangles indicate locations of blowups. (b) Oblique perspective using HiRISE-derived topography (5× vertical exaggeration) looking upslope to the southeast. The light-toned blocks are embayed by the medium-toned blocks and matrix materials within BD. Yellow outlines indicate locations of blowups. Location of topographic profile is noted. (c) Example of alternating light- and medium-toned layers within a fold. Inset shows where small faults displaced the layers after emplacement. Enhanced HiRISE color. (d) Blowup of light-toned outcrop with boulder that has shed off of it (yellow arrow). Enhanced HiRISE color. (e) Blowup of light-toned outcrops embayed by medium-toned blocks. Label and asterisk indicate location where CRISM spectrum was extracted. (f) Example of unit LLM within BD. Inset shows a blowup where dozens of beds are visible in this vertical exposure. Enhanced HiRISE color. (g) Topographic profile showing light-toned outcrops are <10 m in height above medium-toned blocks. (For interpretation of the references to color in this figure legend, the reader is referred to the web version of this article.)

et al., 2005). These valleys have been partially filled in by LD (Fig. 10d), indicating that LD post-dates both ML and any possible fluvial activity along the wallrock.

Other valleys dissecting ML and filled in by LD are observed in the southeast of our study region (Fig. 11). Based upon measurements from a HiRISE DTM, the valleys range from 2 to 4 m deep at the higher elevations and increase in both depth and width downstream towards the south. Unit LD drapes across 4–5° surface slopes and consists of a few layers (Fig. 11b). The deposit is only a few meters thick based upon measurements made using the DTM. ML appears thicker with numerous beds exposed but no evidence of the underlying wallrock except near a steep escarpment (Fig. 11a).

The stratigraphy as observed in a DTM (Fig. 11c) and discussed further in Section 3.3 indicates that ML is dissected by valleys, including drainage networks and meanders (Fig. 11d), and these valleys were subsequently partially infilled by LD. Erosion has removed portions of LD, especially on the highest and steepest hills. Along the geologic contact between LD and ML is a dark outline that can extend upslope into valley-like features (Fig. 11d). The dark outline appears to represent a shallow depression (~2–3 m deep) formed in ML at the contact with LD, similar to a moat.

Please cite this article in press as: Weitz, C.M., et al. Mixtures of clays and sulfates within deposits in western Melas Chasma, Mars. Icarus (2014), http://dx.doi.org/10.1016/j.icarus.2014.04.009

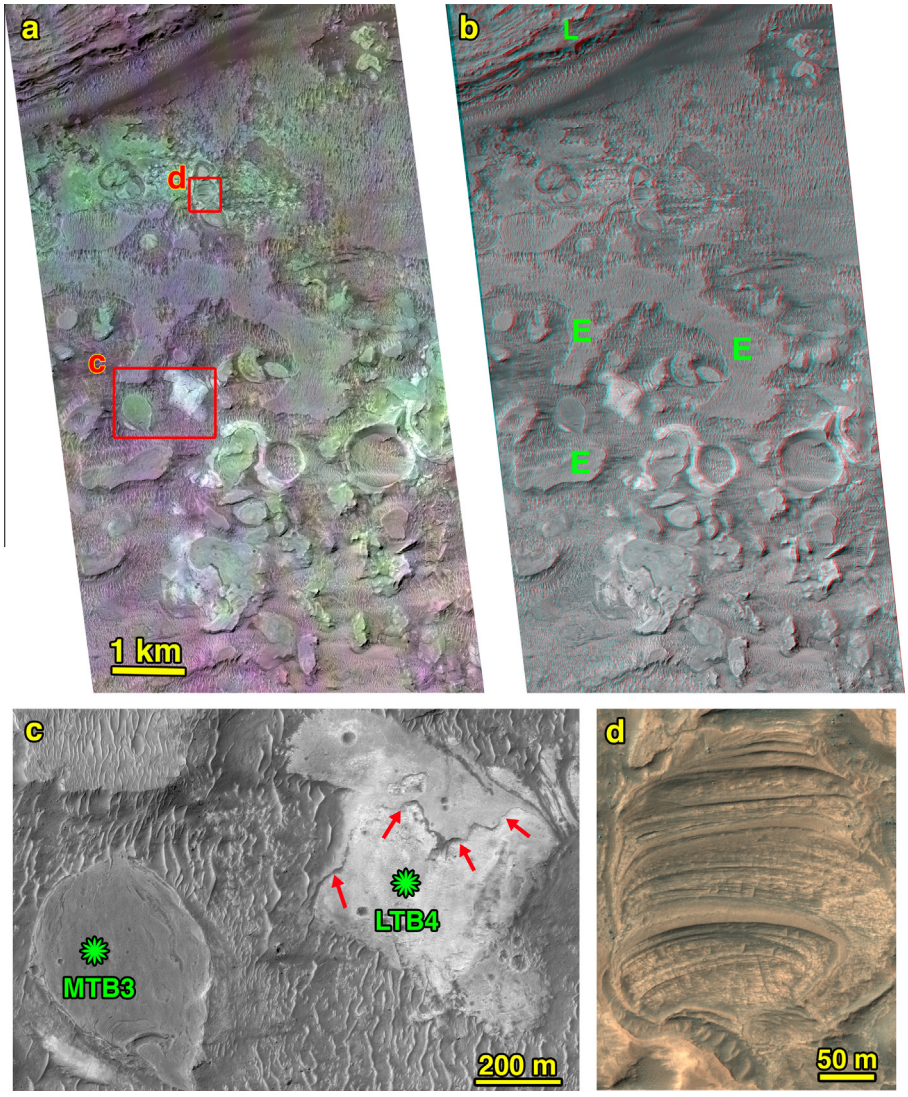

Fig. 7. (a) Portion of HiRISE image ESP_016739_1715 with CRISM FRT00016B12 spectral parameters overlain in color (red is olivine index, green is band depth at 1.9 μm, blue is sulfate index). Medium-toned blocks and matrix within BD are green in color and consistent with polyhydrated sulfates (PHS) while white areas correspond to light-toned irregular blocks that display the 2.28 μm absorption characteristic of nontronite. (b) Stereo anaglyph of blocks within BD, adjacent landslide (L), and mesas of eolian ripples and debris (E). (c) Blowup of medium- and light-toned blocks. Asterisks and labels correspond to CRISM spectra shown in Fig. 13a. Red arrows note the contact with an upper surficial layer on a light-toned block. (d) Blowup of bedding exposed within BD. Enhanced color does not distinguish between the beds, suggesting they are composed of similar materials. (For interpretation of the references to color in this figure legend, the reader is referred to the web version of this article.)

Eolian debris has accumulated within these moats, creating a darker surface. Because the moats are only observed within ML, either ML is weaker and less resistant to erosion than LD or LD has eroded back along this contact to reveal the paleotopography.

LD sometimes displays multiple layers along its edge whereas the interior portions of LD appear to be mixtures of multiple materials based upon lithologic variations (Fig. 12). Mixtures of materials within the LD deposit are also observed in CRISM spectra (see next section). An example of a slightly darker deposit that appears to have slid down onto brighter LD material, as indicated by flow bands and folds, is shown in Fig. 12. The upper darker materials show fainter fracturing relative to the lower brighter deposit (Fig. 12f). Fig. 12 also shows additional moats at the contact between LD and ML. Here, too, the moats represent a depression formed in ML along the contact with LD. A topographic profile across the geologic contact indicates a 6 m drop in elevation going from LD to ML where the dark moat is located (Fig. 12g).

4. Spectral results

We analyzed all the CRISM images shown in Fig. 2a that covered our study region. Spectral parameters were determined for each image, and then spectra were extracted from these images based upon where the parameters showed features of interest. In most cases, the spectral variations seen in CRISM images correlated with morphological differences identified in HiRISE, CTX, and HRSC visible wavelength images.

The wallrock exhibits no obvious hydration features in the 1–2.6 μm region of the spectrum. In addition, CRISM data do not indicate pyroxenes and olivine are present other than in a few small outcrops. Other wallrock exposures in Valles Marineris have been shown to exhibit clay signatures (Murchie et al., 2009b; Roach et al., 2010; Flahaut et al., 2012) and although there could be clays in the Melas wallrock within our study area, the wallrock is covered by eolian debris and mass wasting material, inhibiting our ability to detect any clays.

Please cite this article in press as: Weitz, C.M., et al. Mixtures of clays and sulfates within deposits in western Melas Chasma, Mars. Icarus (2014), http://dx.doi.org/10.1016/j.icarus.2014.04.009

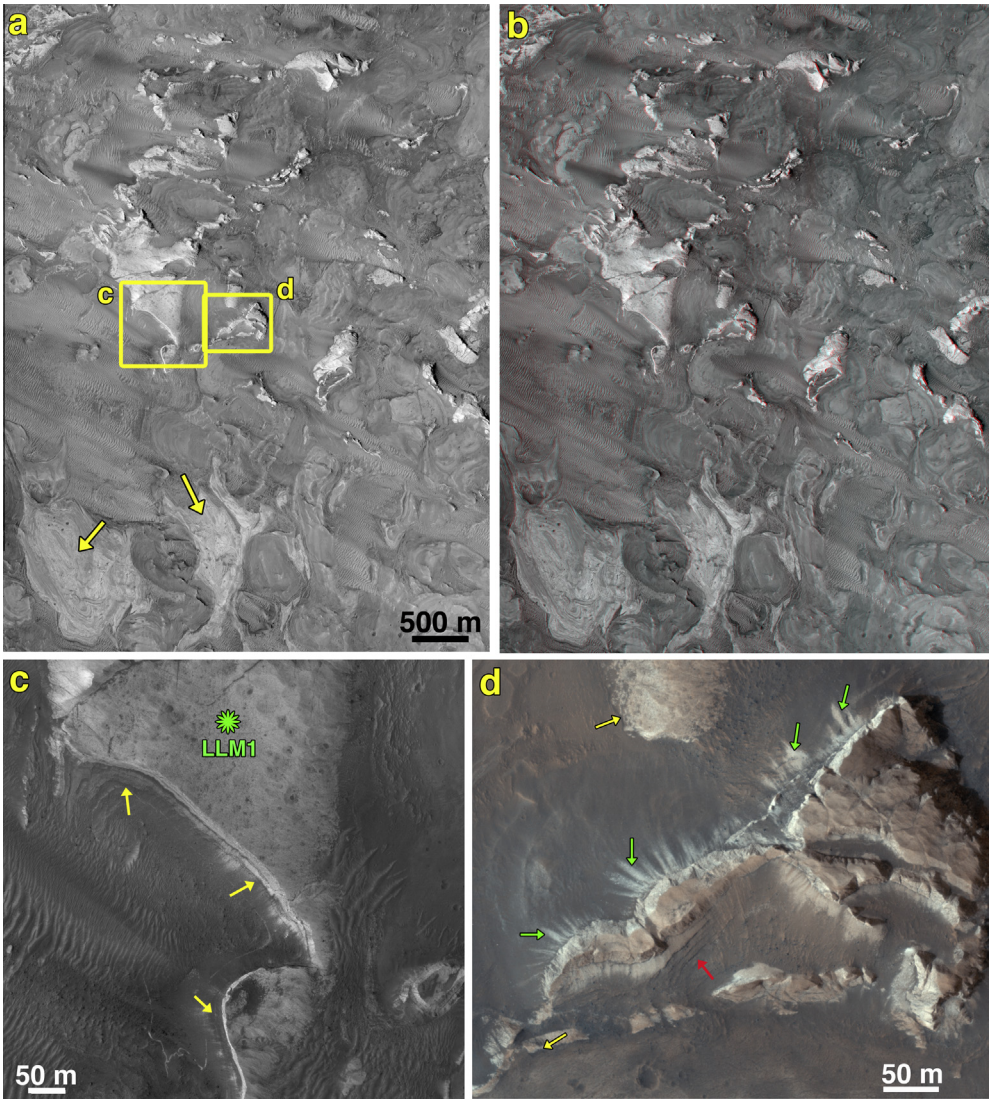

Fig. 8. Examples of unit LLM from HiRISE image ESP_030044_1710. (a) Compared to the light-toned blocks within unit BD (yellow arrows), LLM outcrops appear brighter. Rectangles indicate the locations of blowups. (b) In the stereo HiRISE anaglyph, LLM outcrops are taller and are bounded by steeper escarpments. (c) Several beds are visible within this outcrop (yellow arrows). The upper surface of the outcrop appears smoother and less fractured relative to the light-toned blocks within BD. Green asterisk and label corresponds to CRISM spectrum shown in Fig. 13b. (d) Enhanced color image of LLM rocks showing bedding (red arrow) and talus (green arrows) adjacent to the outcrop where erosion has produced fine debris. Yellow arrows indicate where medium-toned blocks and BD materials can be seen embaying the Ca-sulfate outcrops. (For interpretation of the references to color in this figure legend, the reader is referred to the web version of this article.)

4.1. Floor deposits

Most of the medium-toned blocks within BD are spectrally featureless or display weak hydration signatures around ~1.9 μm. In some instances, the lack of spectral features can be attributed to eolian debris observed along their surfaces. In other cases, the surfaces appear relatively clean (texture can be observed at meter scales), suggesting the surface contains no diagnostic minerals that can be detected with CRISM. Where features are present, the medium-toned blocks display an absorption around 1.94 μm and a shoulder at 2.40 μm (Fig. 13a; MTB1, MTB2), both consistent with a polyhydrated sulfate (PHS). Another weak and broad absorption extending from ~2.14 to 2.33 μm may sometimes be present, suggesting additional minerals may be mixed in with the PHS.

Spectra extracted from two of the light-toned blocks within unit BD (LTB1 and LTB2 in Fig. 4a) have absorptions at 1.92, ~2.21, and 2.28 μm, as well as a shoulder at 2.265 (Fig. 13a). The narrow 2.28 μm feature is best explained by a Fe–OH combination band in the Fe-smectite, nontronite. The 2.21 μm absorption varies in depth and width across the light-toned blocks. Compared to laboratory spectra, the best match could be either an Al-bearing clay, such as montmorillonite, or a hydrated silica. The spectrum for LTB1 shows a broad absorption around 2.21 μm that is not well-matched to the very sharp and narrow laboratory montmorillonite spectrum, suggesting for this block hydrated silica may be a more likely component mixed in with the nontronite. Jarosite can also exhibit an absorption at 2.21 μm but there should be a stronger feature at 2.26–2.27 if it were present. This observation contrasts with doublets noted in spectra from elsewhere in Valles Marineris (e.g. Roach et al., 2010; Weitz et al., 2011, 2012), where a 2.265–2.278, rather than a 2.28 μm feature is observed. Because we observe the 2.28 μm feature in spectra taken from several LTB locations and in multiple CRISM images, we interpret it as nontronite rather than the result of noise, spectral ratios, or other factors associated with CRISM data. Hence, the slightly longer 2.28 μm absorption suggests that at least some nontronite is present in the LTB deposits, along with possible hydrated silica or other mixtures.

Please cite this article in press as: Weitz, C.M., et al. Mixtures of clays and sulfates within deposits in western Melas Chasma, Mars. Icarus (2014), http://dx.doi.org/10.1016/j.icarus.2014.04.009

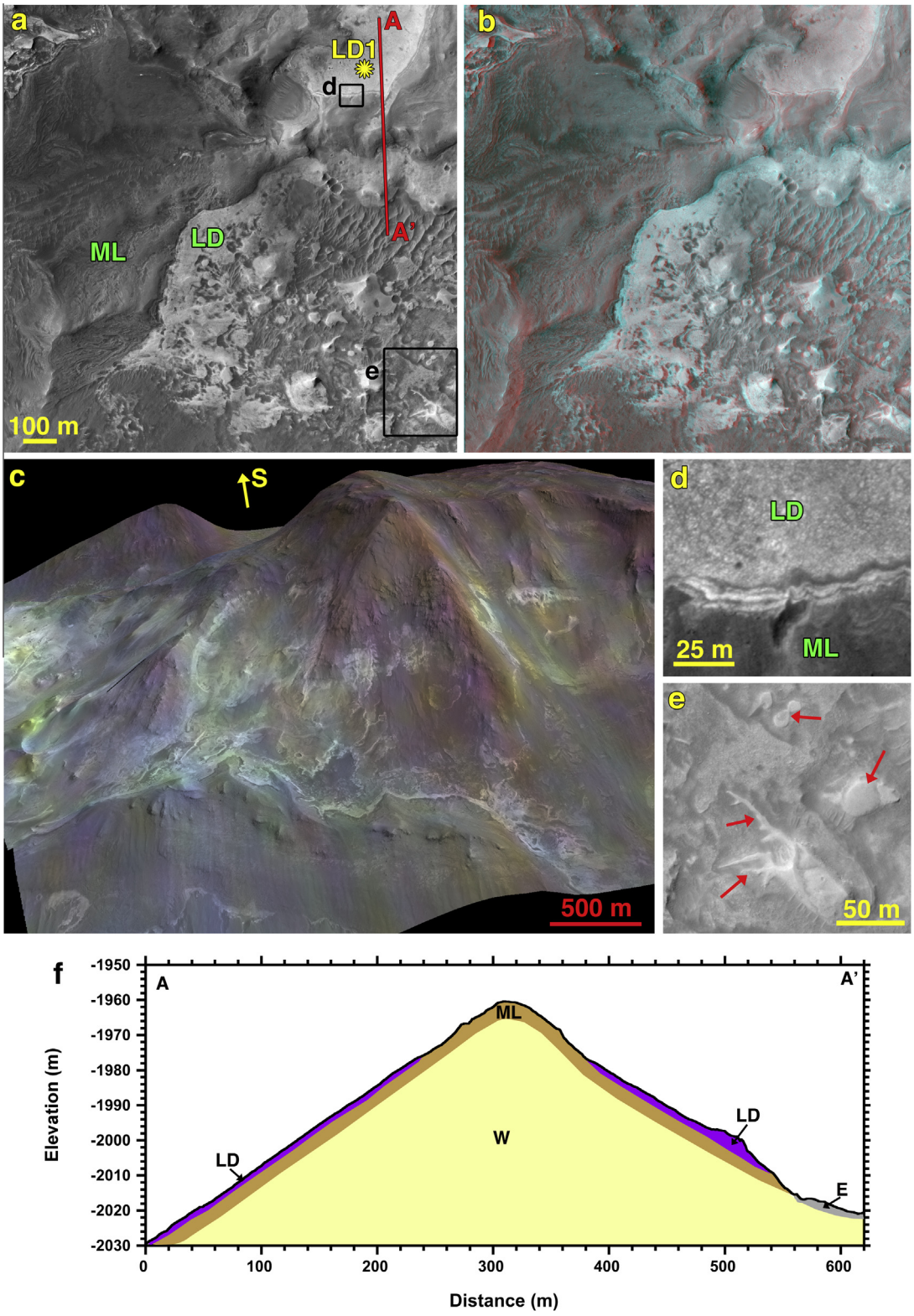

Fig. 9. (a) Portion of HiRISE image ESP_011293_1710 showing units LD and ML draped along southern wallrock slopes above western Melas Chasma. Locations of blowups (black boxes), topographic profile (red line), and CRISM spectrum (yellow asterisk and label) are noted. (b) HiRISE stereo anaglyph showing where unit LD appears along slopes and flat-lying topography. Unit LD lies stratigraphically above ML. (c) Oblique perspective using HiRISE-derived topography (4× vertical exaggeration) merged with CRISM spectral parameters in color (red is olivine index, green is band depth at 1.9 μm, blue is doublet absorption between 2.2 and 2.3 μm). Only unit LD displays hydration features and appears whitish-green in color. ML is seen at all elevations whereas LD is not seen along the higher wallrock surfaces. (d) Multiple layers of variable brightness are visible along the edge of LD. (e) Rounded and branching ridges (red arrows) exhibited within LD. The ridges are a few meters in height while the rounded mound is 7 m high based upon DTM measurements. (f) Topographic profile illustrating stratigraphic relationships between the units. See Fig. 2 for legend of geologic units. (For interpretation of the references to color in this figure legend, the reader is referred to the web version of this article.)

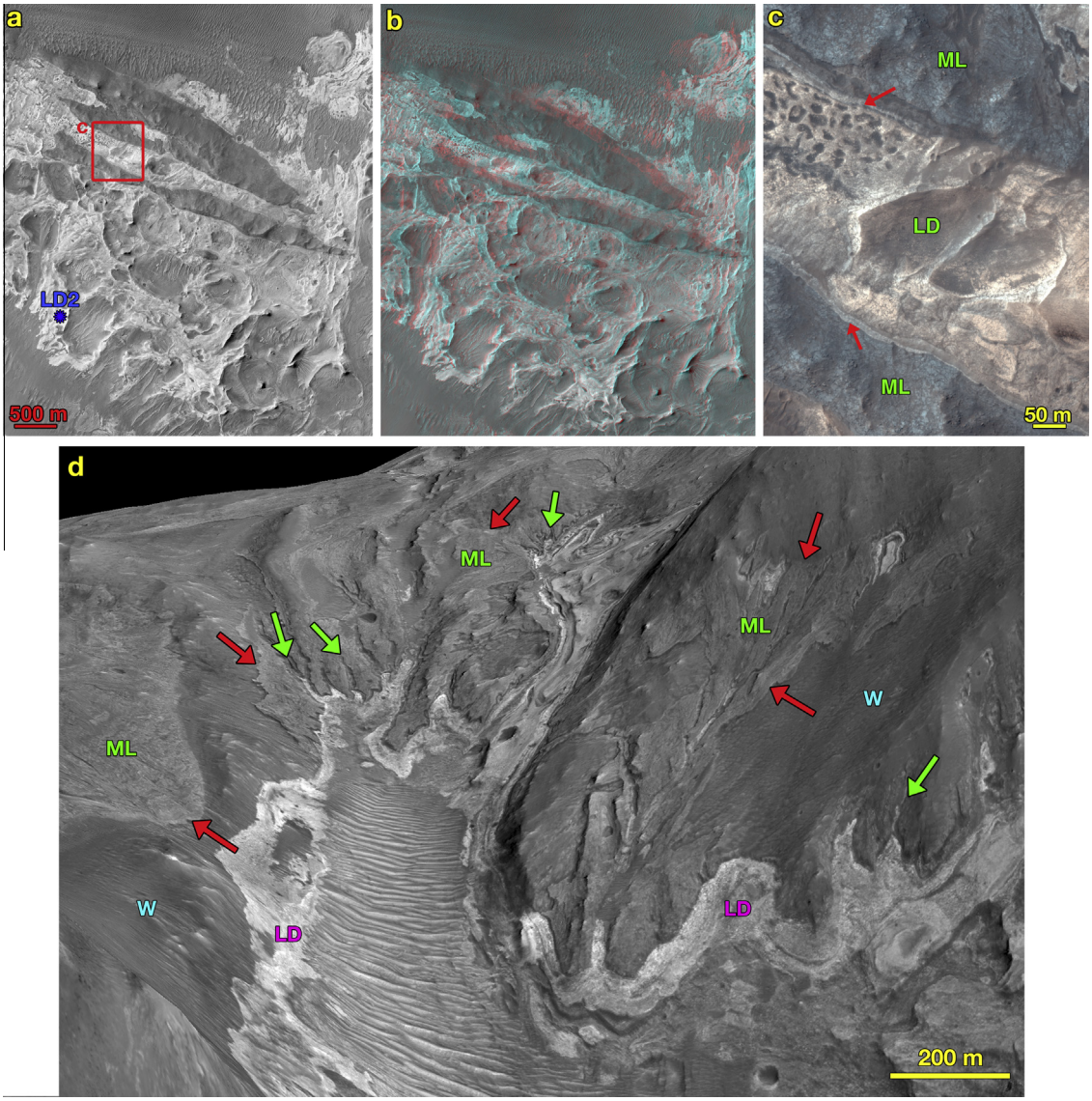

Fig. 10. (a) Portion of HiRISE image ESP_026022_1710 showing light-toned (LD) and medium-toned (ML) deposits draped across the lower wallrock slopes. Blue asterisk and label indicates where CRISM spectrum plotted in Fig. 14a was extracted. (b) In the HiRISE stereo anaglyph, the light-toned deposits are concentrated along shallower slopes and extend onto the adjacent chasma floor, merging with BD materials. (c) Enhanced color image showing several layers within LD (red arrows). (d) Oblique perspective using HiRISE-derived topography looking upslope (southward) at 5× vertical exaggeration. Unit ML is superimposed on the wallrock (W), as indicated by geologic contacts at red arrows. Unit LD covers portions of ML, including filling in valleys that dissect ML (green arrows). (For interpretation of the references to color in this figure legend, the reader is referred to the web version of this article.)

An alternative is that the 2.21 μm feature is caused by K-Jarosite. K-Jarosite exhibits a pair of absorptions at 2.21 and 2.265 μm. If K-Jarosite is present, it would explain the shoulder observed at 2.265 μm. If this is correct, we are then observing a combination of nontronite and jarosite mixed at subpixel scales.

The light-toned block in Fig. 7c has a surficial layer that appears slightly lower in reflectance relative to the underlying material. Erosion of this upper layer has removed it across much of this block. Spectrally, the light-toned block (Fig. 13a, LTB4) exhibits absorptions at 1.92 and 2.28 μm. A CRISM spectrum taken from a light-toned outcrop shown in Fig. 6e (LTB3) has a broad absorption around 1.94 and a shoulder at 2.4 μm matching a PHS, but there are additional weak absorptions between ~2.20 and 2.26 μm.

CRISM spectra extracted from LLM outcrops (Fig. 8) have features with band centers at 1.43, 1.77, 1.92, 2.49, and possibly weak absorptions at 2.23 and 2.27 μm, suggesting the presence of a hydrous Ca-sulfate (Fig. 13b). The 1.43 and sharp 1.92 μm features are more consistent with bassanite, while the weak 2.2 μm features are characteristic of gypsum. Because HiRISE images show bedding occurs at scales smaller than can be resolved in CRISM pixels, it is plausible that both gypsum and bassanite exist in distinct beds but are mixed within any given CRISM spectrum. The two Ca-sulfates could have been deposited at different times, or the gypsum may have changed into bassanite over time by dehydration (Vaniman et al., 2008).

4.2. Wallrock deposits

A CRISM spectrum (LD1) extracted from unit LD at higher elevations (Fig. 9a) is shown in Fig. 14a. The spectrum exhibits weak absorptions around ~1.93 and ~2.27 μm. An additional CRISM spectrum (LD2) extracted from LD at lower elevations (Fig. 10a) appears similar to LD1, with an additional weak absorption at 2.20 μm and 2.40 μm.

Please cite this article in press as: Weitz, C.M., et al. Mixtures of clays and sulfates within deposits in western Melas Chasma, Mars. Icarus (2014), http://dx.doi.org/10.1016/j.icarus.2014.04.009

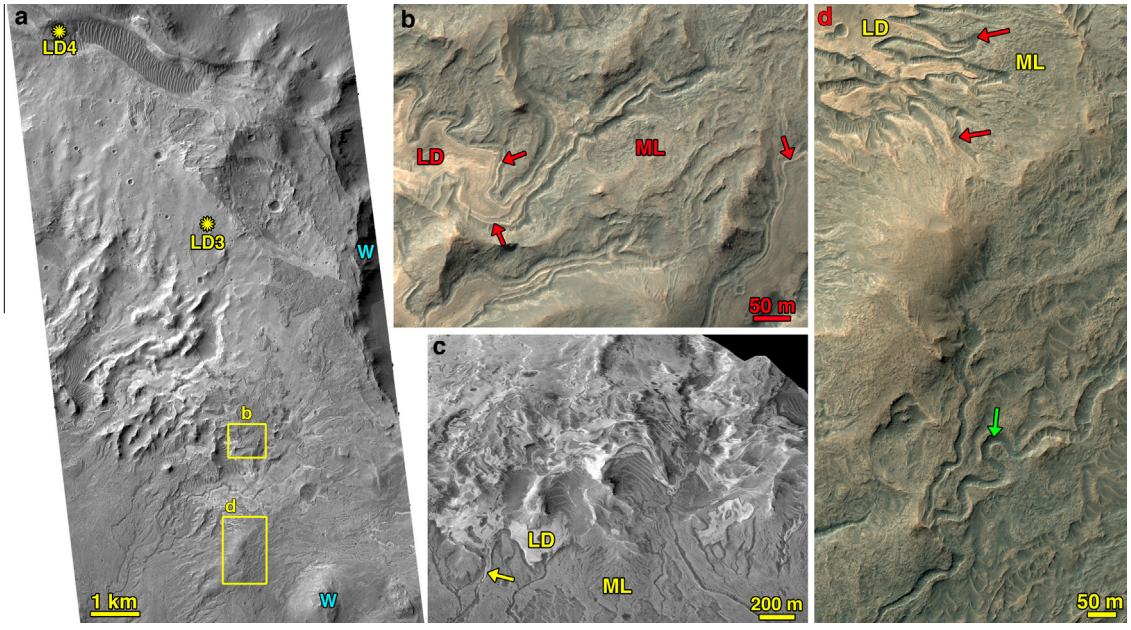

Fig. 11. (a) Portion of HiRISE image PSP_005452_1700. Yellow rectangles indicate locations of blowups while yellow asterisks and labels identify where CRISM spectra were taken. Wallrock (W) is only visible on mounds and the edge of an escarpment. (b) Enhanced color image showing several layers visible in LD (red arrows). Notice the dark 'moat' that follows the geologic contact between LD and ML. (c) Oblique perspective using HiRISE-derived topography (5× vertical exaggeration) looking upslope (northward) along the edge of LD. LD drapes across ML, including along hilly slopes. Numerous valleys dissect ML while LD fills in the upslope portions of these valleys (yellow arrow). (d) Example of a simple symmetrical meander (green arrow) in one of the valleys. Shorter valleys are also seen along the contact between LD and ML (red arrows). Enhanced HiRISE color. (For interpretation of the references to color in this figure legend, the reader is referred to the web version of this article.)

CRISM spectra taken of LD in the southeastern portion of our study region (Fig. 11a) are also plotted in Fig. 14a. LD3 appears similar to previous LD spectra with absorptions at ~2.265 and 1.92 μm, and a break in slope at 2.21 μm. Another spectrum extracted along the walls of an elongated depression (LD4) is unlike the previous LD spectra, with a doublet absorption at 2.21 and 2.28 μm.

In general, we note that portions of LD that are slightly darker-toned (e.g., LD6) exhibit spectra with weakened 2.21 and 2.26 μm features, a 1.9 μm band centered at 1.94 μm, and a shoulder at 2.4 μm. The absorption at 1.94 μm and shoulder at 2.4 μm are consistent with the presence of a PHS. In contrast, the spectra of nearby lighter-toned materials exhibit stronger absorptions at 2.21 and 2.265 μm (LD5) and a shift of the 1.9 μm hydration feature to 1.92 μm, suggesting these deposits lack PHS.

The presence of bands at 1.94, 2.21, and 2.26 μm features could be indicative of a jarosite. Alternatively, the spectrum of the evaporitic residue of acid-treated clays also tends to exhibit a hydration feature at 1.90 μm along with rounded absorptions around 2.21 and 2.26 μm. These 2.21 and 2.26 μm features differ from those of crystalline jarosite in that they are less sharp and appear to be superposed on a broader 2.2 μm feature reminiscent of that exhibited by the spectrum of hydrated silica (Fig. 14a). Hence, the shift of the hydration band from 1.94 to 1.92 μm and the deepening of the 2.2 to 2.26 μm region is consistent with the presence of the evaporitic residue of an acid-leached clay, or perhaps a combination of jarosite and hydrated silica.

4.3. Comparison to other martian spectra

In order to explore our spectra in greater detail, we plotted a blowup of the 1.7–2.6 μm region (Fig. 14b) of several example spectra and compared them to laboratory spectra of minerals with possible matches to these features, as well as similar Mars spectra identified elsewhere. The laboratory spectra of jarosite exhibit an absorption at 2.27 μm that is a possible match to the 2.27 μm features identified in LD spectra. For comparison, we plotted in Fig. 14b a spectrum from Mawrth Vallis which Farrand et al. (2009) identified as a jarosite. Farther to the southeast of our study region and also on the Melas Chasma plateau, small jarosite deposits have been previously identified (Milliken et al., 2008; Metz et al., 2010). Our spectrum extracted from this previously noted plateau jarosite is plotted in Fig. 14b (MP2). Unfortunately, many of our spectra have too much noise and weak absorptions to confidently identify the presence of jarosite. Additionally, there are other absorptions in our spectra that cannot be attributed to jarosite, indicating mixtures are likely present in our deposits. Several LD spectra are similar to the spectrum ATC from an acid-leached Fe-smectite (Madejová et al., 2009) and poorly crystalline Fe–SiO_2 bearing precipitate (Tosca et al., 2008a) produced in the laboratory, suggesting a leached clay may be another phase mixed into our deposits.

We also plot a spectrum of a deposit identified on the floor of Ius Chasma (Roach et al., 2010), just to the west of our study area. The absorptions at 2.21 and 2.27 μm are very similar to those seen in our Melas spectra (Fig. 14b). However, the 1.92 μm hydration band is not as strong as that seen in our Melas spectra. Roach et al. (2010) suggested three possible interpretations to explain their 2.21 and 2.27 μm doublet spectrum from Ius: (1) neoformed precipitates/acid leached smectites; (2) jarosite mixed with an Al–OH phase; and (3) nontronite mixed with an Al–OH phase. Based upon our spectra and these comparisons to laboratory and other martian spectra, we interpret LD to represent similar mixtures of materials to those observed at Ius Chasma, although the lack of an absorption at 2.28 μm for most of the deposits would rule out possibility three. Lithological variations and layering observed in HiRISE images of LD (e.g., Figs. 10c and 12c) are also consistent with mineral mixtures.

5. Stratigraphy

We utilized HRSC and HiRISE DTMs (Fig. 2) in order to determine stratigraphic relationships between the rock types we identi-

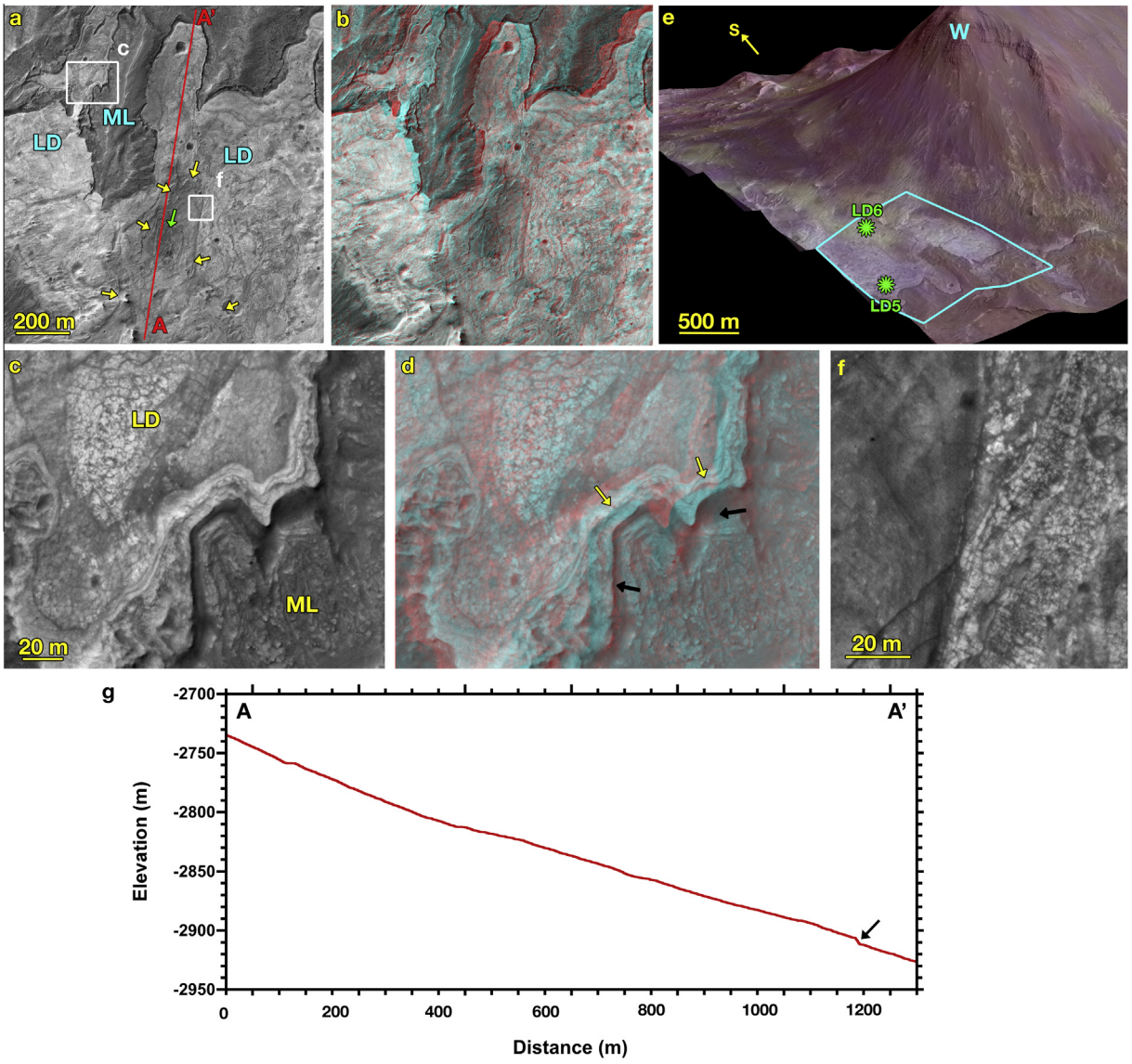

Fig. 12. (a) Portion of HiRISE image PSP_007443_1700 showing units LD and ML. White rectangles indicate locations of blowups while yellow arrows point out the edge of a slightly darker deposit that appears to have been emplaced on to brighter LD material, as indicated by flow bands and folds (green arrow). Location of topographic profile is shown by red line. (b) HiRISE stereo anaglyph of same area. LD drapes across and fills in lower-lying portions of ML. (c and d) The contact between LD and ML has an elongate depression that appears like a moat around LD (black arrows). The edge of LD can display multiple layers, as shown here, that are higher than the interior portions of LD (yellow arrows). Note the heterogeneities in LD lithology, consistent with mixtures of materials in the deposit. (e) Oblique perspective using HiRISE-derived topography at 5× vertical exaggeration with CRISM spectral parameters overlain in color (red is olivine index, green is band depth at 1.9 μm, blue is doublet absorption between 2.2 and 2.3 μm). Unit LD can be subdivided into two mineral phases, where yellow colors indicate a stronger 1.9 μm hydration feature and spectral similarity to PHS whereas whitish colors indicate stronger absorptions at 2.21 and 2.27 μm (see Fig. 14a, LD5 and LD6). Fine layering is visible near the top of a wallrock (W) exposure. Blue outline indicates location of (a). Green asterisks and labels indicate locations where CRISM spectra were extracted. (f) The darker PHS-bearing LD materials do not display the heavily fractured morphology of the brighter LD materials. (g) Topographic profile derived from HiRISE DTM. Black arrow denotes geologic contact and 6 m drop in elevation going from LD to ML at moat. (For interpretation of the references to color in this figure legend, the reader is referred to the web version of this article.)

fied and mapped in this location. Additionally, topographic profiles were extracted from the DTMs and schematic interpretive cross-sections produced. A schematic cross section showing the stratigraphic relationships for the different deposits mapped in our study region is illustrated in Fig. 15 and a table denoting the stratigraphic relationships and inferred mineralogies is given in Table 1. Unit BD is mostly observed along the floor of western Melas Chasma, with some outliers located at higher elevations along lower wallrock materials. Near the central portion of BD, LLM appears in mounds that have been embayed by the younger materials associated with BD. The Ca-sulfates may cover much of the trough floor but only higher-standing exposures are not buried beneath eolian debris and BD materials.

Within BD, light-toned blocks and outcrops (Figs. 6e and 15) are generally embayed by rounded medium-toned blocks or darker matrix materials. The light-toned rocks are only visible where eolian debris and medium-toned blocks have not covered them, which is why they generally appear as higher-standing outcrops. Because the light-toned blocks show flow structures consistent with those also observed in the medium-toned blocks, we interpret them to represent co-eval or slightly older deposits emplaced as part of unit BD, rather than older deposits that formed with the Ca-sulfate LLM deposits. Smaller light-toned outcrops are embayed by the medium-toned blocks and materials within BD (Figs. 5 and 6), indicating an older age. We also observe that there are several medium- and dark-toned materials associated with BD that appear

Please cite this article in press as: Weitz, C.M., et al. Mixtures of clays and sulfates within deposits in western Melas Chasma, Mars. Icarus (2014), http://dx.doi.org/10.1016/j.icarus.2014.04.009

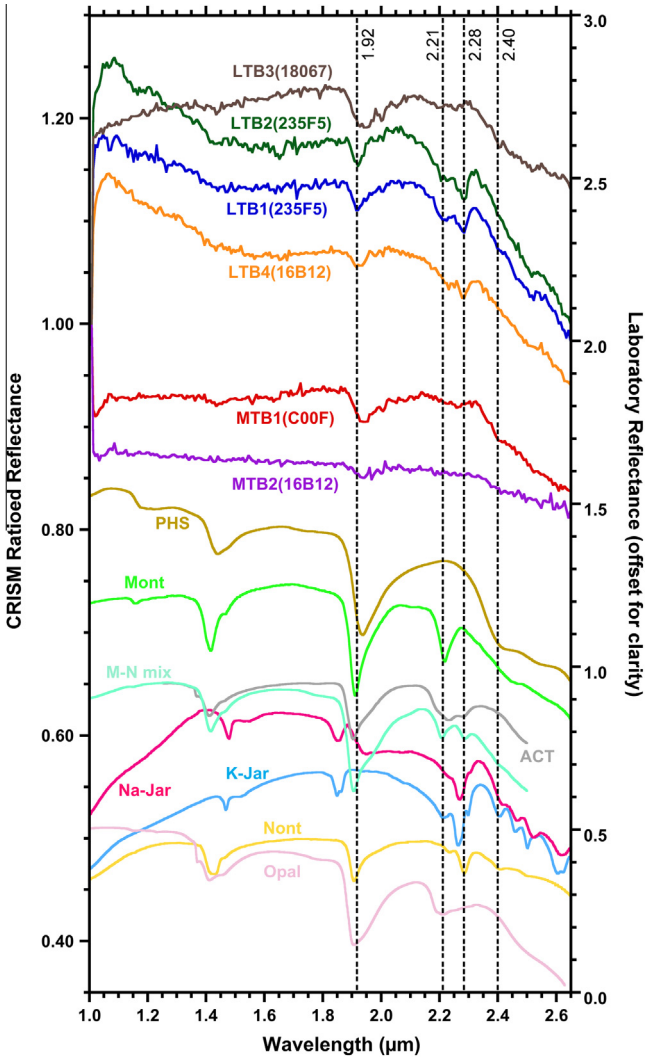

Fig. 13a. Selected CRISM spectra extracted from blocks within unit BD. Labels indicate the CRISM image ID (in parentheses) and the geologic feature from which each spectrum was extracted, where LTB is light-toned block and MTB is medium-toned block (see other figures for locations of spectra). Also shown are laboratory spectra of selected minerals/phases likely present: opal, polyhydrated sulfates (PHS), potassium jarosite (K-Jar), sodium jarosite (Na-Jar), montmorillonite (Mont), nontronite (Nont-0.05), a mixture of montmorillonite and nontronite (M–N mix) and acid-treated clay (ACT+0.3). Medium-toned blocks may have a hydration feature at 1.94 μm and a shoulder at 2.4 μm, consistent with polyhydrated sulfates (PHS). In some of these spectra, an additional unknown mineral appears to produce a weak absorption between 2.2 and 2.3 μm. The light-toned blocks typically have shorter hydration features (~1.92 μm) and a narrow feature at 2.28, consistent with nontronite. Some of these spectra have an additional feature at ~2.21 μm that could be due to hydrated silica (opal), a leached smectite, or an Al-clay.

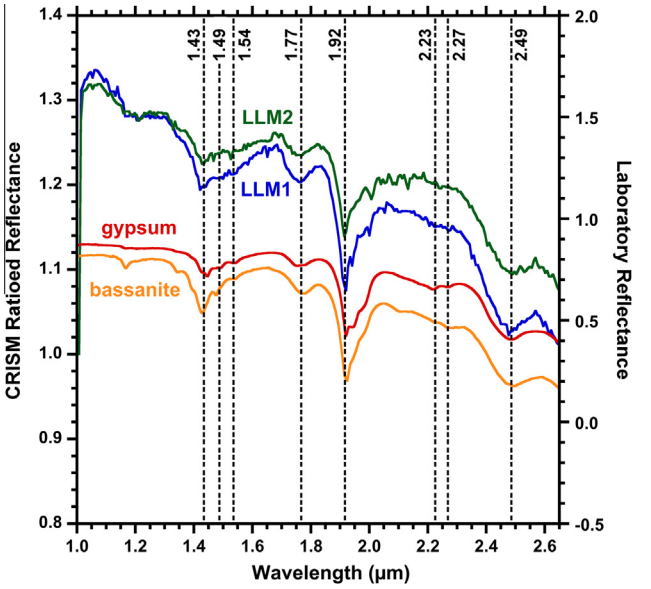

Fig. 13b. CRISM spectra taken from two LLM exposures (see Fig. 8 for location of LLM1; LLM2 was taken from an outcrop where there is no HiRISE coverage). Laboratory spectra of both gypsum and bassanite are shown for comparison.

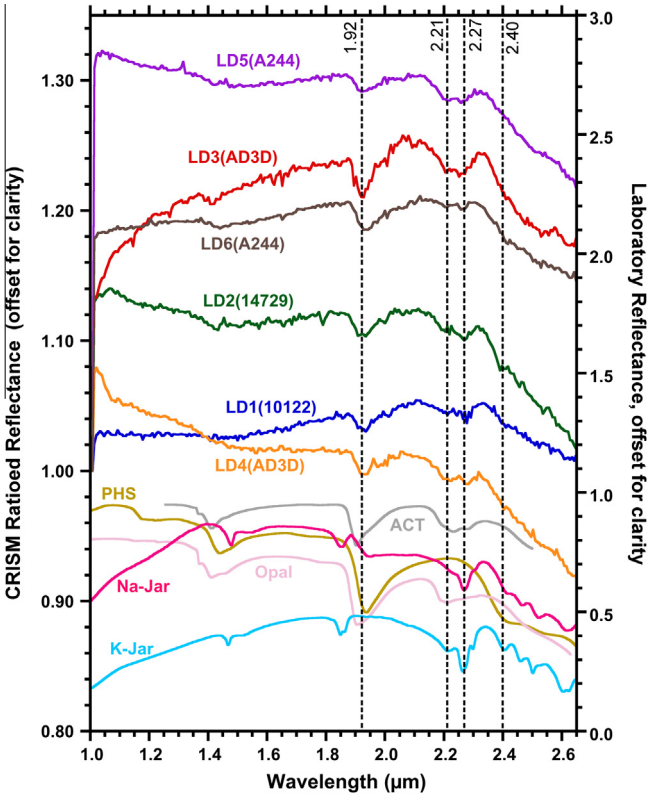

Fig. 14a. CRISM spectra of selected LD deposits. Labels in parentheses indicate the CRISM image from which the spectrum was taken. Some spectra are offset for clarity (LD3+0.05, LD5+0.04). Also shown are laboratory spectra of selected minerals/phases likely present: polyhydrated sulfates (PHS), potassium jarosite (K-Jar-0.2), sodium jarosite (Na-Jar), opal, and acid-treated clay (ACT+0.3).

at stratigraphically different levels, with the dark-toned covering the medium-toned materials. For example, in Fig. 5 a dark-toned material embays a medium-toned material, which in turn embays light-toned outcrops. Based upon these observations, we interpret the light-toned outcrops to represent an older deposit of unknown origin, which was subsequently embayed by medium-toned materials and blocks associated with BD, followed by a younger dark-toned deposit that appears to have flowed down the lower wall-rock slopes. The dark-toned deposit does not extend very far from the wallrock relative to the much larger extent of the medium-toned blocks within BD.

Along the wallrock, ML covers much of the lower slopes (Figs. 2a and 15). At generally lower elevations and draping across portions of ML is unit LD. Based upon both mineralogy and morphology, LD can sometimes be subdivided into darker-toned PHS-bearing and lighter-toned lacking PHS signatures. In general, the PHS-bearing materials tend to be stratigraphically above the

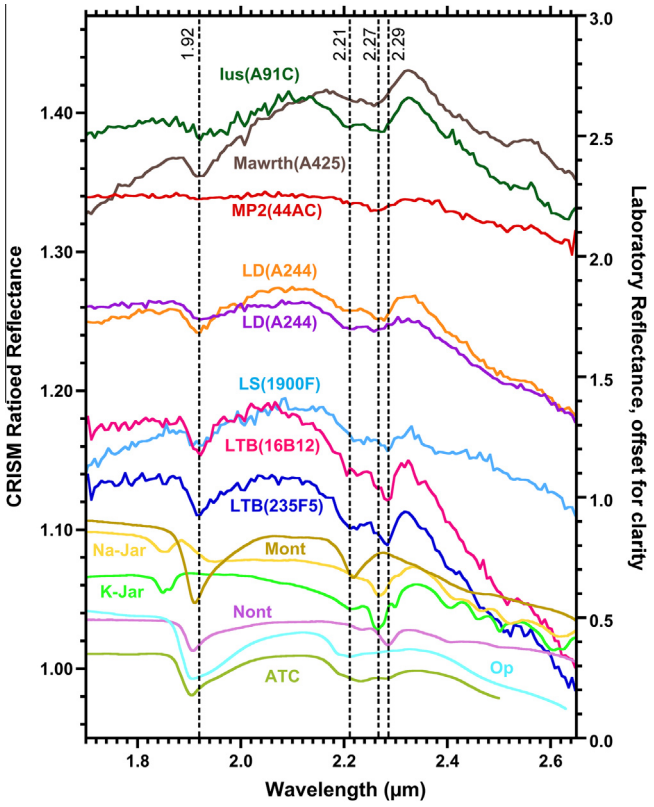

Fig. 14b. Blowup showing the 1.7–2.65 μm region. Light-toned blocks in BD (LTB), light-toned draping (LD), layered sulfates (LS), Melas plateau (MP2) deposit interpreted by Milliken et al. (2008) as jarosite, Mawrth Vallis deposit interpreted by Farrand et al. (2009) as jarosite, and Ius Chasma deposit interpreted by Roach et al. (2010) as a mixture of phases. Labels in parentheses indicate the CRISM image from which the spectrum was taken. Also shown are laboratory spectra of selected minerals/phases with similar features: Potassium jarosite (K-Jar), sodium jarosite (Na-Jar), opal (Op), nontronite (Nont), montmorillonite (Mont) (offset by −0.5) and acid-treated clay (ATC) (offset by −0.3).

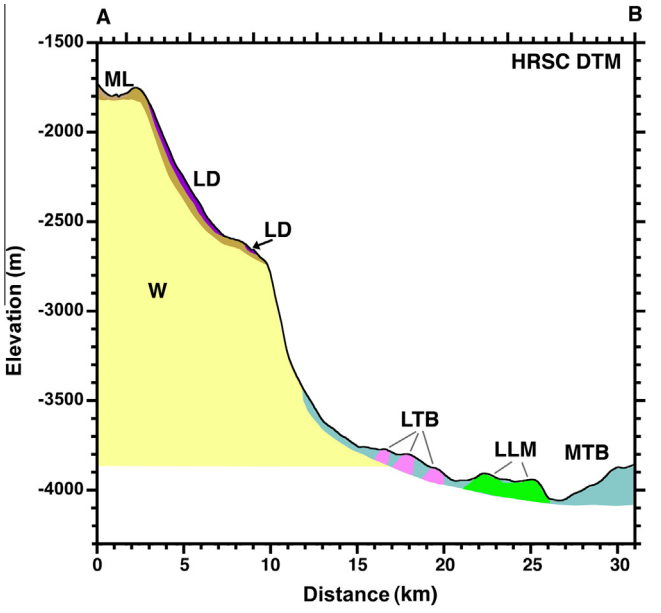

Fig. 15. Interpretive cross-section derived from a HRSC DTM across profile AB shown in Fig. 2a. Three different rock types are classified along the chasma floor: light-toned layered mounds (LLM), medium-toned rounded blocks in BD (MTB), and light-toned irregular blocks in BD (LTB). Other geologic units include wallrock (W), light-toned draping (LD), and medium-toned layered (ML). Thicknesses are not to scale but instead have been vertically exaggerated in order to demonstrate stratigraphic relationships. Contacts below the surface are inferred.

non-PHS-bearing materials within LD (Fig. 12), indicating a younger age of emplacement, although their current stratigraphy may reflect a mass wasting age relationship rather than the original depositional sequence. Because ML covers Melas Chasma wallrock slopes and is dissected by Hesperian age valleys (Quantin et al., 2005) whereas LD fills in these valleys, ML is likely Hesperian in age while LD could be Hesperian in age or younger.

6. Regional geologic setting of the blocky deposit

In order to provide further insight into possible origins for the deposits within our study region, we examined the regional geology of southwestern Melas Chasma (Fig. 16), focusing on the identification of additional hydrated minerals and aqueous landforms that could be related to those within our study region. To the west of our study region, there are additional exposures of both LD and ML along the wallrock slopes in Ius Chasma. To the east, we identified exposures of ML but no exposures of LD. Instead, along the lower wallrock slopes and chasma floor, there are light-toned layered deposits that exhibit spectral signatures of both monohydrated sulfates (kieserite) and PHS (Fig. 17) (Weitz et al., 2013a). HRSC and CTX images show these layered sulfates (LS) occur across much of the Melas chasma floor and lower southern wallrock, but we only identify the specific mineralogy (kieserite or PHS) where there are available CRISM images. Kieserite is generally associated with massive exposures that weather into loose bright boulders, whereas PHS tends to exhibit finely layered and heavily fractured beds (Fig. 18). In Fig. 18c, examples of possible flow features and deformation are visible in the PHS deposit, especially the darker-toned materials, and appear similar to those observed in unit BD (see Fig. 12a).

Based upon stratigraphic relationships derived from a HiRISE stereo anaglyph, the kieserite deposit in Fig. 18 is situated below the overlying PHS deposit. Similar mineralogic sequences that consist of an underlying kieserite and overlying PHS deposit are commonly observed within ILDs in Valles Marineris (e.g., Mangold et al., 2008; Murchie et al., 2009c; Weitz et al., 2012). The PHS consists of interbedded light- and medium-toned layers that exhibit different spectral features (Fig. 18). The spectra of the light-toned layers exhibit a general shape consistent with PHS (Fig. 17, LS5), whereas the medium-toned layers display a broad absorption between 2.16 and 2.33 μm, suggesting additional mixtures (Fig. 17, LS4). Unfortunately, the hyperspectral data taken of this area are noisy, making it difficult to further constrain the mineralogy.

Another region of interest to the southeast of our study area is the Melas basin, a postulated paleolake with layered sediments and deltas that formed in the Late Hesperian from precipitation and/or melting snow (Mangold et al., 2004; Quantin et al., 2005; Metz et al., 2009; Williams and Weitz, 2014). Many of the valleys observed in unit ML of our study region continue downslope and terminate within the Melas basin. Additional valleys are found to the east and also flow into the basin (Quantin et al., 2005; Williams and Weitz, 2014). Metz et al. (2010) identified a small blocky deposit in the northwestern portion of the basin (see Fig. 8 from Metz et al. (2010)) composed of kilometer-scale convoluted folds. CRISM spectra do not exhibit any diagnostic features that would indicate this blocky deposit is related to unit BD based upon mineralogy.

While the Melas basin has numerous layered sediments and fan-shaped landforms (Williams and Weitz, 2014), there is very limited evidence for hydrated minerals. Metz et al. (2010) identified a possible jarosite at one location within the basin (Fig. 16),

Table 1
Stratigraphic relationships and inferred mineralogies.

Unit	Overlies	Underlies	Inferred mineralogy
Blocky deposit (BD)	LLM	–	–
Medium-toned rounded blocks (MTB)	(Subunits in BD;		Polyhydrated sulfates
Light-toned irregular blocks (LTB)	MTB overlies LTB)		Fe/Mg smectites, and/or Al-smectites, hydrated silica, jarosite
Light-toned layered mounds (LLM)	–	BD	Gypsum and/or bassanite
Light-toned draping deposit (LD)	ML, W	–	Jarosite, and/or hydrated silica, pre-cursor clays, residue of acid-treated clay. PHS may also be present
Medium-toned layered deposit (ML)	W	LD	–
Wallrock (W)	–	ML, LD	–

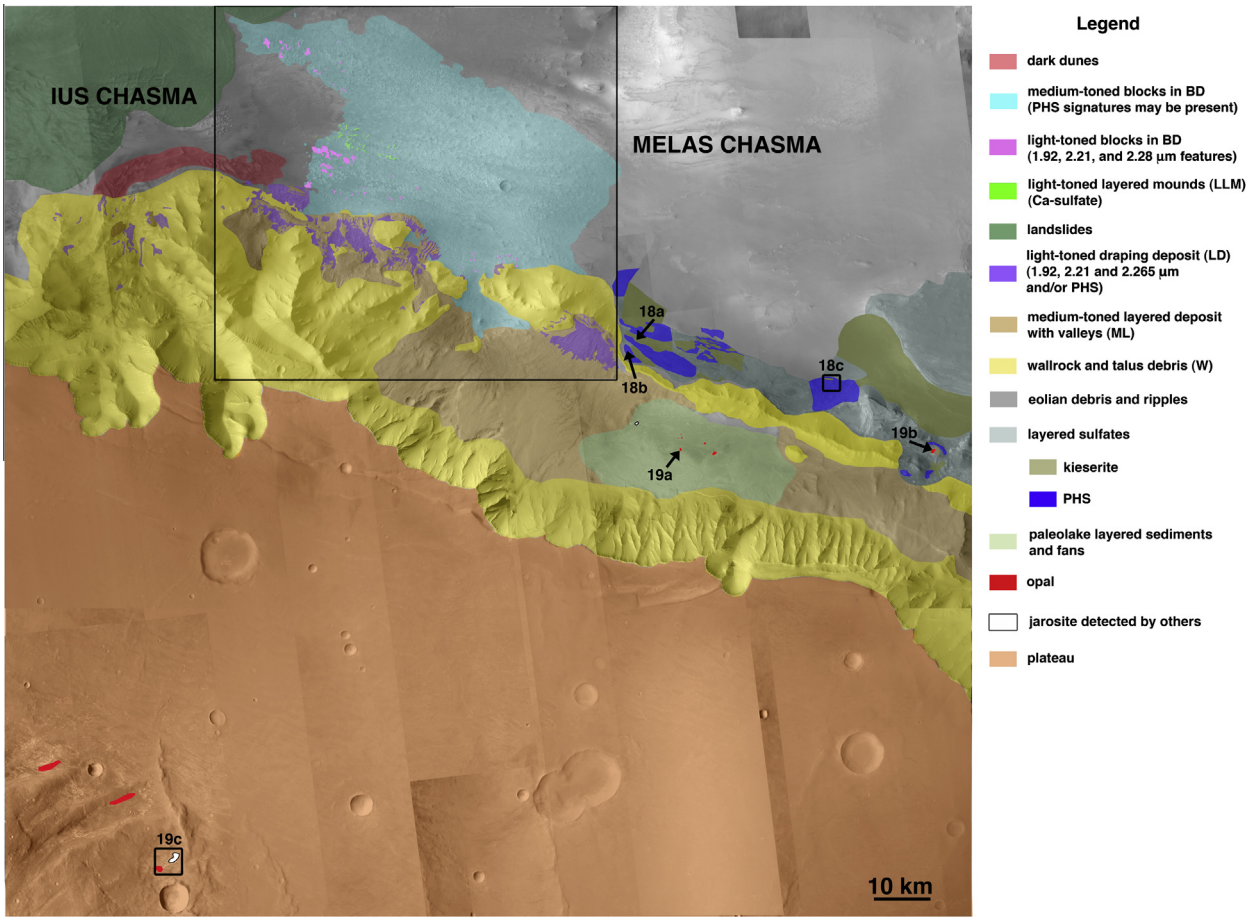

Fig. 16. Regional geology of southwestern Melas Chasma, with the study area outlined by large black box. Later figures are identified by arrows and small black boxes. CTX images overlain on THEMIS daytime IR mosaic.

while Metz et al. (2010) and Williams and Weitz (2014) found several spots where opal was detected in CRISM images (Fig. 16). A CRISM spectrum extracted from one of the opal sites (Fig. 19a) is plotted in Fig. 20 (MB1), with broad absorptions centered at 1.93 and 2.21 μm. Because hydrated silica can occur in several degrees of crystallization (i.e., opal-A, opal-CT), the position of the 2.21 μm absorption shifts to slightly different wavelengths depending upon the crystallinity (Milliken et al., 2008).

An additional spot of opal is mapped farther east within LS (Fig. 16). Although the CRISM data are relatively noisy for this image, the spectrum exhibits absorptions at ~1.41, 1.93, and 2.21 μm (Fig. 20, MB2), consistent with opal. The opal corresponds to light-toned materials along the edge of a mound (Fig. 19b). Compared to the LD unit in our study region, this hydrated silica exposure appears thicker and massive, and also lacks the 2.2–2.3 μm doublet.

Finally, along the Melas Chasma plateau to the south of our study region, additional hydrated minerals and valley networks, including inverted channels, have been observed (Milliken et al., 2008; Weitz et al., 2010; Le Deit et al., 2010). Opal and jarosite identified in CRISM data are associated with light-toned layered deposits along the plateau. In CRISM spectra, the opal deposit (Fig. 20, MP1) is similar to those identified in the Melas basin and to the east. In HiRISE images (Fig. 19c), the opal deposit appears darker and heavily pitted relative to these other opal exposures, however. The spectrum interpreted by Milliken et al. (2008) as a Fe-deficient H_3O-bearing jarosite (Fig. 19c) is plotted in Fig. 14b (MP2). Because these plateau deposits are >80 km in

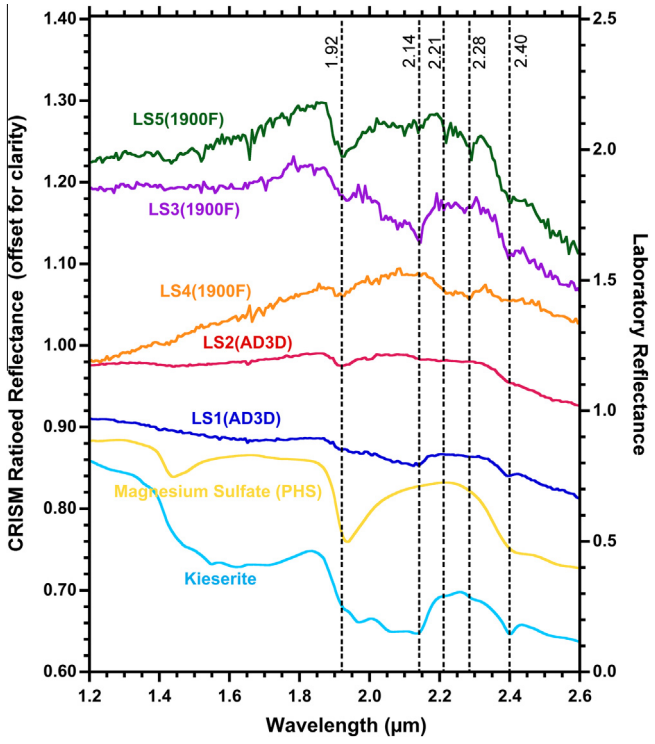

Fig. 17. CRISM spectra extracted from the layered sulfates (LS) unit. Labels in parentheses indicate the CRISM images from which the spectrum was taken. Spectra LS4 (1900F) is offset for clarity (−0.1). Also shown is a laboratory spectrum of kieserite and magnesium sulfate. CRISM image HRL1900F is a lower spatial resolution image and has considerably more noise than FRTAD3D.

distance and display lithologies unlike those observed within our study region, we suggest they formed under environmental conditions and by processes that are unique to the geologic setting along the plateau rather than what we observe along the Melas wallrock and chasma floor, as discussed more in the next section.

7. Discussion

7.1. Formation of deposits along wallrock slopes

Based upon our CRISM analyses and those by Roach et al. (2010), the most likely phases in LD include mixtures of jarosite, acid-leached clays (yielding silica), primary precipitates (silica, poorly crystalline clays), and/or PHS. The possibility that the ferric sulfate mineral jarosite is present within unit LD would require an acidic, wet, and oxidizing environment, with a pH < 4 (Stoffregen et al., 2000; King and McSween, 2005), while the leached smectite and hydrated silica would also support an acidic environment. At Meridiani Planum where jarosite has been identified *in situ* from rover measurements (Squyres et al., 2004; Klingelhöfer et al., 2004), the jarosite is interpreted to have formed in acid-saline shallow waters. Jarosite and bassanite have been detected at Mawrth Vallis (Noe Dobrea et al., 2011; Farrand et al., 2009; Wray et al., 2010) while both gypsum and jarosite have been identified from CRISM data in Noctis Labyrinthus troughs (Weitz et al., 2011; Thollot et al., 2012).

The jarosite identified by Milliken et al. (2008) along the Melas Chasma plateau is associated with light-toned layered deposits that are thought to have formed by evaporation of fluids that resulted from acidic dissolution of basalt in the Late Hesperian to Amazonian. The jarosite detected in the Melas basin to the east is thought to be a cement formed at low temperatures, perhaps as pore fluids in sediments that were deposited within a paleolake (Metz et al., 2009). At Mawrth, the strongest jarosite signature comes from an ovoid-shaped depression where acidic, sulfur-rich water may have ponded and precipitated jarosite (Farrand et al., 2009), but it is also found in variable abundances throughout the Al-phyllosilicate-bearing unit in what was potentially an acid-pedogenic environment (Noe Dobrea et al., 2011). Neither of these two geologic settings applies to the LD deposits we have identified along the Melas wallrock.

Laboratory experiments under ambient martian conditions (Madden et al., 2004) indicate that chemical weathering of basalt can form jarosite. The jarosite may have resulted from either a large amount of water altering only a thin outer layer of rock or more abundant quantities of rock partially weathered by a small amount of water (Madden et al., 2004). If the water is not removed quickly then the pH will increase and jarosite will no longer be the dominant Fe-sulfate to precipitate. This type of alteration may provide a more consistent source of jarosite formation along the southwestern Melas wallrock.

Just to the west along the Ius chasma floor, Roach et al. (2010) identified a light-toned deposit with a 2.21 and 2.27 μm doublet, similar to many of the spectra taken from Melas (see Fig. 14b). Roach et al. (2010) suggested the deposit, which they referred to as a hydrated silicate, was only a few meters thick and deposited on both sulfates and Fe/Mg-smectites. They also identified the hydrated silicate in landslides. Because the Ius hydrated silicate is spectrally and morphologically similar to the deposits we have identified at Melas, and both deposits are spatially close in Valles Marineris, we interpret LD to be the same hydrated silicate identified in Ius Chasma and also refer to it as a hydrated silicate.

Acid-leached Fe/Mg-smectites that yield amorphous silica or primary precipitates composed of silica and poorly crystalline clays may also be present in LD based upon our CRISM analyses. Altheide et al. (2010) showed that acid-treating of smectites can reduce spectral contrast and shift the positions of metal–OH absorptions in their spectra, a process inferred to explain some spectra in the Mawrth Vallis region (Noe Dobrea et al., 2011) and in/near Endeavour Crater (Noe Dobrea et al., 2012) that exhibit features similar to LD spectra. Roach et al. (2010) suggested acid-leached clays resulting in silica and poorly crystalline clays could explain the hydrated silicate in Ius Chasma that extends into our Melas study region.

The PHS found mixed together or stratigraphically above the hydrated silicate portions of LD indicates a sulfate of unknown cation (possibly Mg or Fe; Ca or Na would be spectrally distinct). On Earth, PHS typically forms as evaporites in standing bodies of water, by acid fog alteration of primary minerals, or by precipitation from saturated groundwater (Settle, 1979; Spencer, 2000). The lack of any monohydrated minerals in the CRISM data indicates the PHS did not convert to a monohydrated phase, such as kieserite, through burial diagenesis or increasing temperatures (e.g., Roach et al., 2009). Because both the PHS and hydrated silicate are found draped across wallrock summits, it seems likely that they formed in place. However, the evidence for flow structures within the deposits suggests they originally formed along the wallrock and then later some of them slid downslope, perhaps as the result of creep or a triggering event (i.e. seismic activity, impact) (Metz et al., 2010). The observation that LD appears as branching ridges could indicate that chemical weathering has affected this deposit. Alternatively, physical erosion may have created the rounded morphologies and branching ridges as a result of differential weathering due to variations in cementation.

Superposition results from our stratigraphic interpretations suggest the hydrated silicate (LD) formed initially, followed by PHS. This is geochemically possible if all the iron had been used

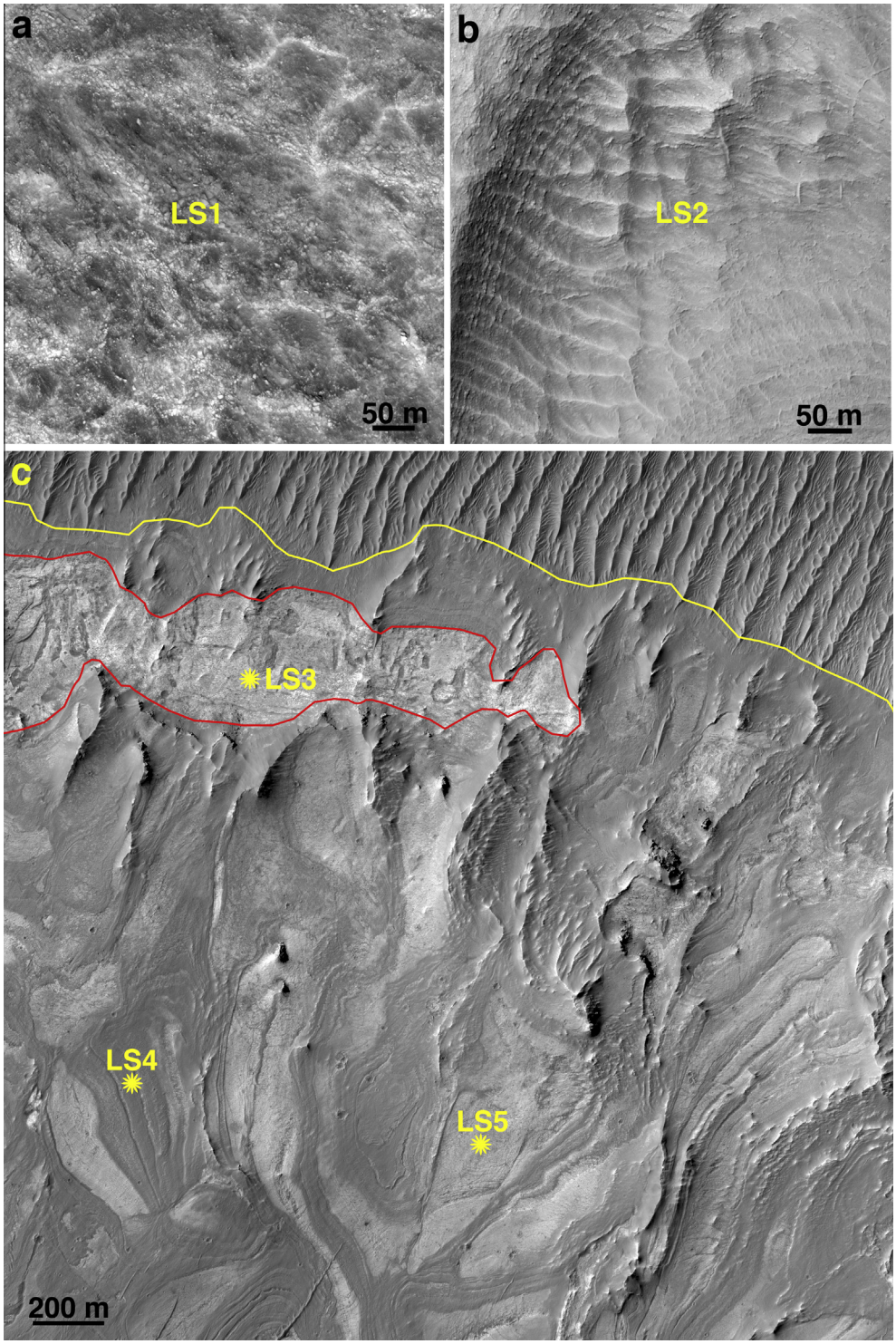

Fig. 18. Examples of kieserite and PHS rocks seen in the layered sulfate unit to the east of our study region. (a) Kieserite is associated with massive exposures that weather into loose bright boulders. CRISM spectrum LS1 was taken from this location. Portion of HiRISE image ESP_31178_1705. (b) PHS is associated with finely layered deposits that are heavily fractured. CRISM spectrum LS2 was taken from this location. Portion of HiRISE image PSP_8735_1700. (c) Contact between underlying kieserite (red outline) and overlying PHS deposit. The PHS consists of multiple layers of variable reflectance and lithology. Possible deformation features are visible in the PHS deposit, especially the darker-toned materials, and appear similar to those seen in unit BD. Yellow asterisks identify locations where CRISM spectra were extracted and plotted in Fig. 17. Portion of HiRISE image ESP_17952_1700. (For interpretation of the references to color in this figure legend, the reader is referred to the web version of this article.)

up to make any Fe-phases, leaving behind magnesium to form the PHS. Alternatively, jarosite is highly insoluble and would precipitate out of dilute fluids whereas Mg-sulfates are more soluble and thus can be more easily concentrated into a brine (Tosca et al., 2008b), resulting in an increase in salinity as the water froze or evaporated. To form the sulfates along the wallrock, liquid water must have been present but only for a short period of time in an arid environment. While today in Valles Marineris water ice is not present for extended periods, ice was likely stable during periods of higher obliquity (Vaniman et al., 2006; Vaniman and Chipera, 2006) and could have supplied the water if portions of the ice melted.

Please cite this article in press as: Weitz, C.M., et al. Mixtures of clays and sulfates within deposits in western Melas Chasma, Mars. Icarus (2014), http://dx.doi.org/10.1016/j.icarus.2014.04.009

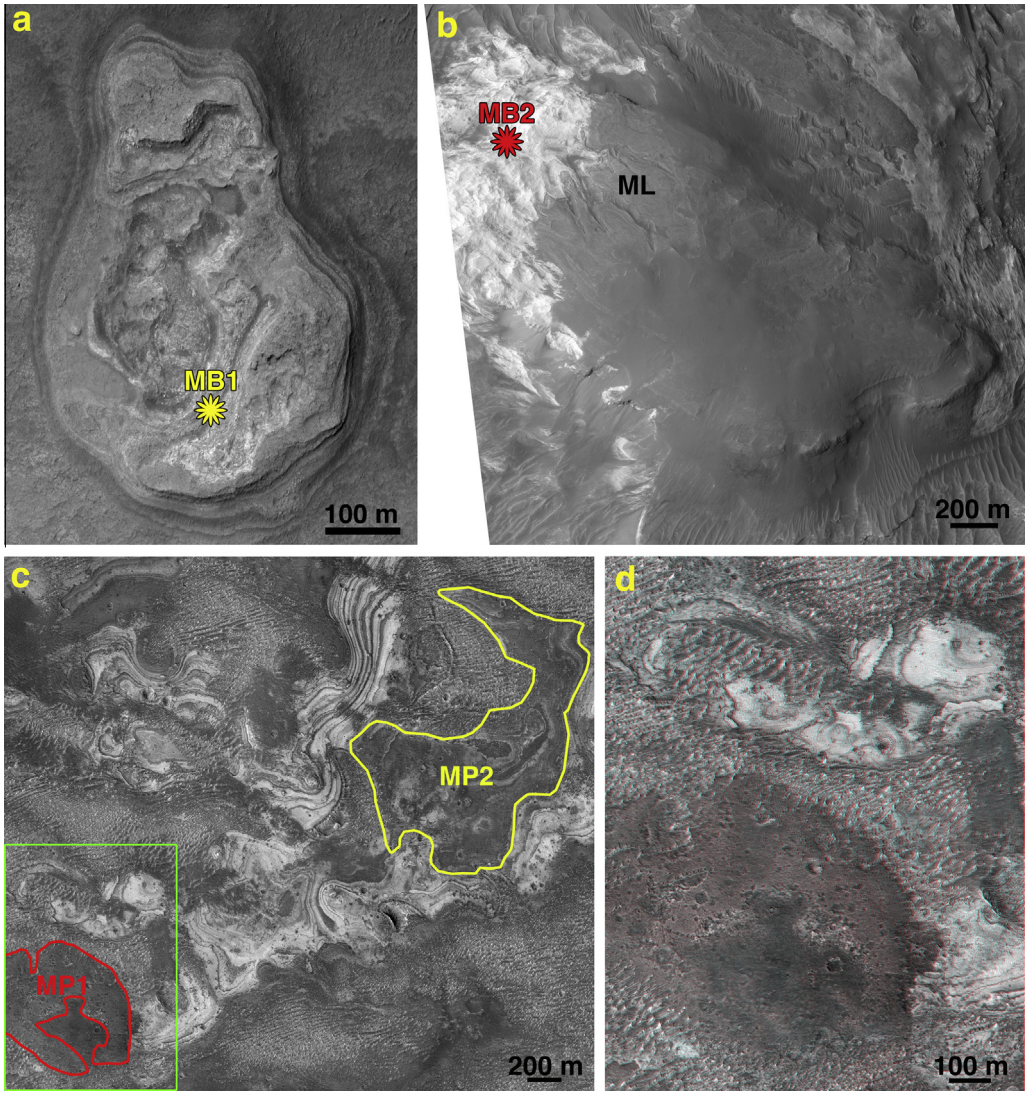

Fig. 19. Examples of opal and plateau deposits. (a) A mound of layered deposits within the Melas basin. Opal corresponds to the brighter materials on exposed layers. Yellow asterisk shows where CRISM spectrum (MB1) was extracted and plotted in Fig. 20. Portion of HiRISE image PSP_7087_1700. (b) The massive light-toned rocks exposed along the edge of a mound in the far eastern portion of Melas basin contains opal. Red asterisk identifies where a CRISM spectrum (MB2) was extracted and plotted in Fig. 20. Portion of HiRISE image ESP_011504_1700. (c) Alternating light- and dark-toned beds are observed in deposits along the Melas Chasma plateau. In CRISM data, the opal corresponds to the deposit outlined in red (MP1) while the material proposed as jarosite by Milliken et al. (2008) is outlined in yellow (MP2). Portion of HiRISE image PSP_3118_1690. (d) In a HiRISE stereo anaglyph, the opal is associated with a medium-toned pitted unit superimposed over older rocks, including the layered beds and jarosite-bearing layer. (For interpretation of the references to color in this figure legend, the reader is referred to the web version of this article.)

Possible origins for the hydrated silicate–PHS mixtures in LD include: (1) in association with atmospheric precipitation that created the valleys (Quantin et al., 2005); (2) alteration of sulfur-bearing volcanic ash; (3) ice or snow along the wallrock slopes that trapped dust and volcanic aerosols (Michalski and Niles, 2012); or (4) groundwater transportation and deposition. Based upon our stratigraphic analyses, the precipitation that created the valleys in unit ML took place before deposition of the LD mixtures, ruling out origin one. The precipitation likely resulted in chemical alteration of materials within ML, yet the lack of any hydrous spectral features within ML suggests this weathering did not produce detectable amounts of hydrous minerals, perhaps because the water quickly percolated into the subsurface or was transported downstream. Alternatively, if ML experienced substantial exposure to liquid water then any soluble minerals would leach out and be transported away, leaving behind rocks free of alteration.

A groundwater upwelling model has been proposed as a method for trapping, cementing, and lithifying layers of eolian dust and sand in Valles Marineris, Meridiani Planum, and Aram Chaos (Andrews-Hanna et al., 2007; Andrews-Hanna and Lewis, 2011; Murchie et al., 2009c). This model is able to reproduce many of the observed deposits, both in size and spatial distribution. Thollot et al. (2012) proposed that basaltic bedrock and volcanic ash deposited within a Noctis Labyrinthus trough were altered by warm acidic groundwater to produce a large number of minerals. The Melas sulfates occur along wallrock slopes but not within a basin that could confine such groundwater, making this an unlikely scenario to explain the sulfates in our study region. Moreover, groundwater would tend to follow pre-existing topography and preferentially fill in low regions, but we observe LD on ridgelines and other elevated terrain.

The draping aspect of LD, especially those outcrops seen near the top of some wallrock exposures, is most consistent with an air-fall origin, such as volcanic ash or atmospheric dust. Such a deposit may be altered by interaction with acidic water before or subsequent to its deposition. Although there is no evidence for a volcanic

Please cite this article in press as: Weitz, C.M., et al. Mixtures of clays and sulfates within deposits in western Melas Chasma, Mars. Icarus (2014), http://dx.doi.org/10.1016/j.icarus.2014.04.009

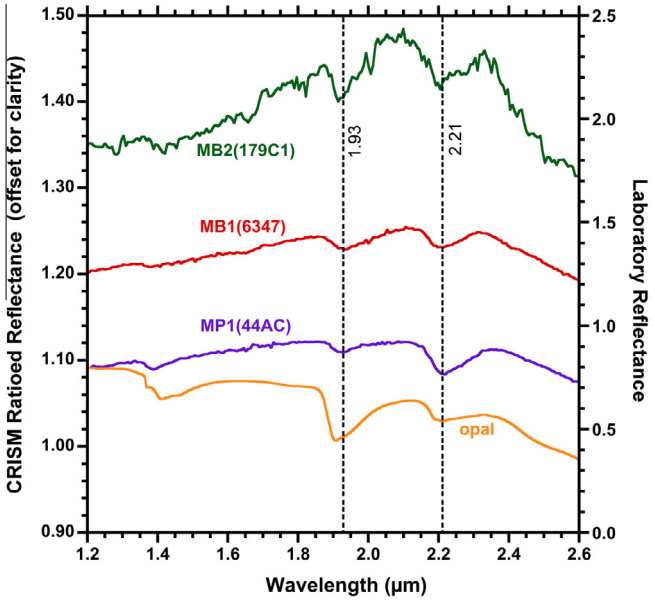

Fig. 20. CRISM spectra of selected opal deposits in and around the Melas basin (MB) and along the Melas plateau (MP). Labels in parentheses indicate the CRISM image from which the spectrum was taken. Spectra MB (179C1) is offset for clarity (−0.4). Also shown is a laboratory spectrum of opal.

vent within Melas, there are numerous linear and rounded depressions, as well as fractures and faults, along the wallrock that may have vented sulfur-rich gases. The interaction of these sulfur-rich gases with water vapor released from these same vents or nearby ice could have generated acidic water capable of altering the deposit and leading to the precipitation of the hydrated silicate initially, followed by Mg-sulfates as the pH increased by titration with the rock. Similarly, airfall deposition of atmospheric dust followed by *in situ* alteration of the dust could potentially explain the phases within LD, although we would expect to see LD spread across many other chasmata wallrock slopes if the deposit resulted from global dust deposition, unless the alteration was localized to the southern walls of Melas and Ius chasmata. The concentration of valley networks at this location seems to indicate unique and favorable conditions for aqueous activity that could alter airfall deposits along the wallrock here relative to the other chasmata.

A model proposed to explain the ILDs within Valles Marineris, as well as the sulfate deposits at Meridiani Planum and other locations on Mars, also requires volcanic aerosols and ice (Niles and Michalski, 2009; Michalski and Niles, 2012). The model proposes acid-weathering inside massive ice–dust deposits that incorporated large amounts of volcanic sulfur gases. These massive dust–ice deposits formed through precipitation of ice condensed around dust grains and acidic aerosols during periods of high obliquity, resembling the polar layer deposits that exist today on Mars. Although this model was suggested to explain the massive sulfate deposits, it is possible that the same processes may occur in thinner and smaller deposits as well, such as those within our study region. The LD unit appears to be only a few meters thick, so perhaps several meters of ice may have been sufficient both to trap volcanic aerosols and dust, as well as allow weathering to create the hydrated silicate and PHS. If ice accumulation was preferentially along wallrock slopes and summits, then the ice could trap airborne dust or volcanic ash particles and favor sedimentation at these same locations. Hence, sedimentation would depend on areas of ice accumulation. However, the observations that a dense valley network and persistent lacustrine body of water existed along the southern wallrock during the Late Hesperian (Mangold et al., 2004; Quantin et al., 2005; Williams and Weitz, 2014) suggest that water was plentiful in this region, perhaps initially in the form of precipitation (rainfall or snow that later melted) to incise the valleys.

7.2. Formation of the chasma floor deposits

A simple explanation for the blocky deposit is that it represents mixtures of LD and ML materials from the wallrock slopes that were moved down onto the Melas Chasma floor. The presence of PHS in both LD and BD deposits is consistent with this hypothesis. However, LD lacks the 2.28 μm nontronite signature observed in the light-toned blocks of BD, whereas BD lacks the 2.265 μm feature seen in LD spectra. The nontronite in BD may have been derived from weathered wallrock that was transported to the chasma floor during formation of the blocky deposit, or the alteration may have occurred during this transport and deposition onto the floor. Additionally, any nontronite that was not transported down to the chasma floor may have been altered under more acidic conditions to jarosite and/or leached clays along the wallrock slopes.

Roach et al. (2010) identified Fe/Mg-smectites along both the wallrock and the floor of Ius Chasma, just to the west of our study area in Melas. They suggested the smectites originally formed in the wallrock and were later transported by mass wasting down to the chasma floor where they accumulated as layered deposits. The nontronite mixtures in Melas are also consistent with mass wasting from the wallrock to the chasma floor, not as fines that were laid down to form sedimentary layered deposits but instead as larger detached slabs of materials within BD. Stratigraphic relationships indicate the PHS-bearing blocks in BD superpose outcrops of the light-toned nontronite mixtures. If the blocky deposit represents multiple episodes of mass wasting, then the nontronite mixtures were laid down initially followed by later deposition of the PHS and spectrally bland medium-toned blocks. Because there are no valleys or other fluvial features associated with the blocky deposit, an origin by fluvial transport seems unlikely. Moreover, we expect that fluvial transport of materials down the wallrock slopes should have destroyed the blocks in BD that we now observe on the chasma floor. Assuming LD was once more extensive across much of the southern wallrock in our study region, then its current patchy appearance could be explained by mass wasting to form BD along the chasma floor, removing much of unit LD along the wallrock.

The Ca-sulfate mounds identified near the center of the blocky deposit (LLM) are the only known occurrence of this phase in central Valles Marineris. Other orbital detections of gypsum on Mars include the walls of Columbus crater (Wray et al., 2011), troughs of Noctis Labyrinthus (Mangold et al., 2010; Weitz et al., 2011, 2013b), the north polar sand dunes on Mars (Langevin et al., 2005; Fishbaugh et al., 2007; Masse et al., 2011) and perhaps Mawrth Vallis and Meridiani Planum (Noe Dobrea et al., 2011, 2012). Gypsum has been found in some rocks and soils of the Columbia Hills in Gusev crater (Squyres et al,, 2006; Yen et al., 2008), and in veins at Endeavour and Gale Craters by the Opportunity and Curiosity rovers, respectively (Squyres et al., 2012; Vaniman et al., 2013).

On Earth, Ca-sulfates are a common sedimentary mineral found in evaporite beds (e.g. Prothero and Schwab, 2004). Gypsum generally forms at temperatures below 60 °C (e.g. Conley and Bundy, 1958) and at higher temperatures will convert to bassanite. Bassanite has also been shown to transition to gypsum when the bassanite nanocrystals become oriented (Van Driessche et al., 2012). Under current martian conditions, gypsum is resistant to dehydration unless it was exposed to higher temperatures that allowed bassanite to form (Robertson and Bish, 2013). Because we observe several beds within the Ca-sulfate outcrops and the CRISM spectra

Please cite this article in press as: Weitz, C.M., et al. Mixtures of clays and sulfates within deposits in western Melas Chasma, Mars. Icarus (2014), http://dx.doi.org/10.1016/j.icarus.2014.04.009

show features consistent with both gypsum and bassanite, the minerals may either have formed concurrently or some of the gypsum later dehydrated to bassanite. Alternatively, the spectra could just represent bassanite or gypsum, rather than a mixture. Stratigraphic relationships between LLM and BD indicate the Ca-sulfates represent older deposits. They could have formed from water infiltration along the chasma floor, perhaps during limited groundwater upwelling (Andrews-Hanna et al., 2007; Andrews-Hanna and Lewis, 2011) that enabled sedimentary deposition of these layered beds in Ca-rich fluids at an earlier stage of brine evolution when fluids were relatively dilute (Tosca et al., 2008b).

7.3. Relationships to deposits around the study region

The opal and jarosite identified along the plateau to the south of our study region (see Fig. 19c) may have formed concurrently with LD, but do not share physical or spectral properties that would support they resulted from the same aqueous conditions. The opal identified on the plateau does not display the doublet at 2.2–2.3 μm seen in LD spectra. It corresponds to a medium-toned deposit that lies stratigraphically above interbedded light-and medium-toned deposits of unknown mineralogy that are not observed in association with LD.

The opal signature detected in the eastern portion of the Melas basin (Fig. 19b) corresponds to a light-toned and massive unit whereas the six opal spots found within the Melas basin appear light-toned and post-date finely layered lacustrine sediments. The Melas basin opal outcrops appear to either represent a younger alteration of pre-existing sediments or deposition of younger materials, likely unrelated to the lacustrine activity within the basin (Williams and Weitz, 2014). Based upon these observations, we propose each opal deposit formed with a unique morphology characteristic of its localized geologic setting. Although spectra for LD and BD can exhibit a 2.21 μm absorption that may be attributed to opal or another hydrated silica, all of these LD and BD spectra also exhibit additional features indicating the presence of other phases and a more complex depositional sequence.

Because the overall mineralogy and morphology of the layered sulfates (LS) in the east are different from that observed within BD or LD (i.e., kieserite + PHS mixtures in LS compared to jarosite, nontronite, and PHS mixtures in BD and LD), and moreover they are spatially separated, we do not believe the layered sulfates were deposited concurrently or by similar processes to either BD or LD. However, the flow and deformation patterns shown in Figs. 6, 12, and 18c all appear similar, suggesting folding and/or displacement of the PHS deposits along the wallrock may have occurred concurrently at both locations. Additionally, the medium-toned upper deposits identified in Fig. 18c exhibit a broad absorption from 2.1 to 2.3 μm, which occurs at the same wavelengths where materials in both LD and BD exhibit absorption features. Hence, we cannot rule out the possibility that some of the younger upper deposits in LS formed coevally and by similar processes to those identified in our study region.

Liu et al., 2013 suggested the layered sulfates in Melas were formed by repeated fluvial events that deposited sediments later altered with rising ground water and evaporation. Monohydrated and polyhydrated sulfates identified along perched basins in the wallrock of Coprates Chasma to the east have been attributed to fluvial events washing aerially deposited ash or dust down the wallrock where it collected within each catchment area (Fueten et al., 2011). Monohydrated sulfates and PHS are commonly observed within the ILD mounds along the floors of many chasmata within Valles Marineris (e.g., Chojnacki and Hynek, 2008; Murchie et al., 2009c; Roach et al., 2009; Bishop et al., 2009; Weitz et al., 2012). The interbedding of kieserite and PHS could reflect variable geochemistry, such as kieserite deposited during highly saline conditions whereas PHS was deposited from more dilute waters (Tosca et al., 2008b). Changes between kieserite and PHS have also been explained in ILDs in Candor Chasma through increased pressures and temperatures converting PHS to monohydrated sulfates during burial diagenesis (Roach et al., 2009). However, because we see distinct layers within the layered sulfates consisting of either kieserite or PHS, it is difficult to explain these alternating hydration states by conversion over time.

Because the geochemistry, morphology, stratigraphy, and spatial distribution of the layered sulfates in southern Melas Chasma are different from the sulfates in our study region, we do not believe they formed from the same processes. Rather, the layered sulfates likely formed by processes similar to those already proposed for the ILDs found in many of the chasmata and discussed previously.

7.4. Sequence of events

Based upon our morphologic, mineralogic, and stratigraphic observations, we suggest the following sequence of events to explain the formation of the light-toned hydrated units in the southwestern Melas Chasma region:

(i) The Ca-sulfate deposits in unit LLM were emplaced in the Hesperian after the Melas Chasma trough floor had formed. LLM may have been deposited in association with evaporation during groundwater upwelling events in Ca-rich waters. The LS unit was deposited in association with ILD deposition across Melas Chasma. Mixtures of kieserite and PHS in LS suggest variable humidity and/or temperatures during deposition and are consistent with similar sulfate mixtures observed in the ILDs of many other chasmata. Units LLM and LS may have been deposited concurrently if Ca-rich fluids were concentrated towards the western portion of our study region while Mg/Fe-rich fluids were located to the east.

(ii) Deposition of ML along wallrock slopes in the Hesperian. The absence of hydration features in CRISM spectra of ML could indicate that water was not involved in deposition and/or alteration of these layered deposits. The draping properties of ML support an airfall origin, perhaps by volcanic ash or atmospheric dust concentrated in this region.

(iii) Formation of valleys in ML during the Late Hesperian (Quantin et al., 2005) and associated downstream deposition of sediments in the Melas basin paleolake that were sourced by these valleys. Williams and Weitz (2014) postulate that there were several periods of lacustrine activity spanning centuries to millennia within the Melas basin associated with precipitation and/or snow melting.

(iv) Deposition of LD along the wallrock, infilling some valleys within ML. The deposition occurred across Ius and western Melas, indicating widespread but limited aqueous activity and alteration to explain the hydrated minerals identified within LD. The draping nature of these deposits is most consistent with an airfall origin (atmospheric dust or volcanic ash), perhaps along the wallrock slopes where ice/snow accumulated and could trap the airborne particles.

(v) Deformation and transport of materials along the wallrock to form light-toned blocks in BD containing nontronite mixtures, followed by medium-toned PHS-bearing or spectrally featureless blocks that embay the light-toned blocks and LLM. Our observations suggest multiple mass movement events spaced out over time to explain the different materials and stratigraphic relationships.

(vi) Small opal outcrops in and around the Melas basin and also on the Melas plateau appear unrelated and likely reflect younger localized aqueous activity during the Late Hesperian to Amazonian.

Please cite this article in press as: Weitz, C.M., et al. Mixtures of clays and sulfates within deposits in western Melas Chasma, Mars. Icarus (2014), http://dx.doi.org/10.1016/j.icarus.2014.04.009

8. Conclusions

Thanks to extensive targeting and numerous images collected over long-term observations of the southwestern Melas Chasma region, we have identified several episodes of aqueous activity spanning from the Hesperian into the Early Amazonian that resulted in deposition and/or formation of hydrated minerals. The chasma floor deposits are dominated by a blocky deposit that consists of mixtures of rounded medium-toned blocks and irregular light-toned blocks. Most of the medium-toned blocks exhibit no spectral features but some have signatures that suggest the presence of PHS. The light-toned blocks exhibit spectral features consistent with mixtures of nontronite and perhaps a hydrated silica, montmorillonite, or an acid leached clay. Nontronite is commonly seen in wallrock exposures of Valles Marineris (Murchie et al., 2009b; Flahaut et al., 2012), but is not observed in our study region. Either the nontronite is obscured by eolian and mass wasting debris along the wallrock, or it is not present in the wallrock at this location.

The blocky deposit displays folds and plastic deformation structures consistent with previous mass wasting origins (e.g., Weitz et al., 2003; Metz et al., 2010) suggesting movement of materials along the southern wallrock and onto the chasma floor. While some of the materials within the blocky deposit may have originated from these wallrock slopes, such as the PHS, the nontronite either represents materials derived from altered wallrock that is not observable today, or it formed during the transport and subsequent deposition of unit BD, representing relatively late clay formation that appears uncommon on Mars (Bibring et al., 2006; Ehlmann et al., 2011). The blocky deposit embays mounds of layered Ca-sulfates along the chasma floor, indicating the Ca-sulfates represent an older unit that may have formed as evaporitic deposits from the ponding and evaporation/freezing of upwelling groundwater.

The deposits observed along the wallrock slopes are an older medium-toned layered unit and a younger thinner light-toned unit. The medium-toned layered deposit does not exhibit any mineralogically diagnostic spectral features and it has been dissected in locations by Late Hesperian-age valleys (Quantin et al., 2005). The younger light-toned deposit is superimposed on the medium-toned unit and can sometimes be seen filling in portions of the valleys, indicating the deposit formed after the precipitation that created the valleys. The light-toned deposit exhibits spectral features consistent with mixtures of jarosite, acid-leached clays, silica, and/or poorly crystalline clays. In some deposits, a PHS signature is also detected in stratigraphically higher darker-toned materials. The doublet absorption between 2.2 and 2.3 μm commonly observed in spectra from LD has also been seen in spectra extracted from deposits in nearby Ius Chasma (Roach et al., 2010). The spatial proximity and similar lithologies of these hydrated silica deposits in Melas and Ius indicate they are likely related deposits. The draping nature of both LD and ML, along with their occurrence along ridgelines and wallrock summits, favors an airfall origin for these deposits, either by volcanic ash or atmospheric dust. Ice/snow accumulation along these wallrock slopes may have influenced and controlled sedimentary deposition by trapping the ash or dust.

Our observations of deposit mineralogy and morphology suggest that environmental conditions along the Melas plateau were unlike those within the chasma. The layered deposits formed within a postulated Melas basin lacustrine environment are unique to this depositional setting and do not share the mineralogy or morphology of the deposits we observe along Melas wallrock exposures. The layered sulfates to the southeast of our Melas study region are comprised of both kieserite and PHS. This mineralogy and their distribution and connection to ILDs farther east within Melas suggest the environment in which the ILDs formed must have been intrinsically different and unrelated to the environment in which the deposits within our study region formed. However, an upper deposit in LS displays both spectral features and morphologies consistent with observations for LD and BD, suggesting either a similar regional deposit was laid down and/or coeval deformation occurred in both regions. The diversity of hydrated minerals within southwestern Melas Chasma indicates numerous distinct and localized aqueous environments, suggesting a complex hydrologic regime existed in this region, perhaps related to a more widespread period of aqueous activity that spanned from the Hesperian into the early Amazonian (Fassett and Head, 2008; Grant and Wilson, 2011, 2012; Howard and Moore, 2011; Weitz et al., 2013).

Acknowledgments

Funding for this project was provided by grants from the NASA Mars Data Analysis Program (NNX08AL14G) to PI Weitz. Additional funding was provided to Weitz as a Co-I on the HiRISE science team. We thank D. Berman for production of the HiRISE DTMs used in this study while the HRSC DTM is courtesy of *HRSCview*, Freie Universitaet Berlin and DLR Berlin, http://hrscview.fu-berlin.de/. J. Bishop kindly provided the spectrum for ATC. A. Baldridge performed initial CRISM analyses on some TRR2 images. This paper benefitted from very helpful reviews by M. Chojnacki and P. Niles on a later version of this manuscript, and J. Flahaut and an anonymous reviewer on an earlier version of this manuscript.

References

Altheide, T.S., Chevrier, V.F., Noe Dobrea, E., 2010. Mineralogical characterization of acid weathered phyllosilicates with implications for secondary martian deposits. Geochim. Cosmochim. Acta 74 (21), 6232–6248.

Andrews-Hanna, J.C., Lewis, K.W., 2011. Early Mars hydrology: 2. Hydrological evolution in the Noachian and Hesperian epochs. J. Geophys. Res. 116, E02007. http://dx.doi.org/10.1029/2010JE003709.

Andrews-Hanna, J.C., Phillips, R.J., Zuber, M.T., 2007. Meridiani Planum and the global hydrology of Mars. Nature 446, 163–168. http://dx.doi.org/10.1038/nature05594.

Andrews-Hanna, J.C., Zuber, M.T., Arvidson, R.E., Wiseman, S.M., 2010. Early Mars hydrology: Meridiani playa deposits and the sedimentary record of Arabia Terra. J. Geophys. Res. 115, E06002. http://dx.doi.org/10.1029/2009JE003485.

Bibring, J.-P. et al., 2006. Global mineralogical and aqueous Mars history derived from OMEGA/Mars Express data. Science 312, 400–404.

Bishop, J.L. et al., 2009. Mineralogy of Juventae Chasma: Sulfates in the light-toned mounds, mafic minerals in the bedrock, and hydrated silica and hydroxylated ferric sulfate on the plateau. J. Geophys. Res. 114, E00D09. http://dx.doi.org/10.1029/2009JE003352.

Catling, D.C., Wood, S.E., Leovy, C., Montgomery, D.R., Greenberg, H.M., Glein, C.R., Moore, J.M., 2006. Light-toned layered deposits in Juventae Chasma, Mars. Icarus 181, 26–51.

Chapman, M.G., Tanaka, K.L., 2001. Interior trough deposits on Mars: Subice volcanoes? J. Geophys. Res. 106 (E5), 10087–10100.

Chojnacki, M., Hynek, B.M., 2008. Geological context of water-altered minerals in Valles Marineris, Mars. J. Geophys. Res. 113. http://dx.doi.org/10.1029/2007JE003070.

Christensen, P. et al., 2004. Mineralogy at Meridiani Planum from the Mini-TES experiment on the Opportunity rover. Science 306, 1733–1739.

Conley, R.F., Bundy, W.M., 1958. Mechanism of gypsification. Geochim. Cosmochim. Acta 15 (1–2), 57–72.

Ehlmann, B.L. et al., 2011. Subsurface water and clay mineral formation during the early history of Mars. Nature 479, 53–60. http://dx.doi.org/10.1038/nature10582.

Farrand, W.H., Glotch, T.D., Rice, J.W., Hurowitz, J.A., Swayze, G.A., 2009. Discovery of jarosite within the Mawrth Vallis region of Mars: Implications for the geologic history of the region. Icarus 204, 478–488. http://dx.doi.org/10.1016/j.icarus.2009.07.014.

Fassett, C.I., Head, J.W.I., 2008. Timing of martian valley network activity: Constraints from buffered crater counting. Icarus 195, 61–89. http://dx.doi.org/10.1016/j.icarus.2007.12.009.

Fishbaugh, K.E., Poulet, F., Chevrier, V., Langevin, Y., Bibring, J.-P., 2007. On the origin of gypsum in the Mars north polar region. J. Geophys. Res. 112, E07002. http://dx.doi.org/10.1029/2006JE002862.

Flahaut, J., Quantin, C., Clenet, H., Allemand, P., Mustard, J.F., Thomas, P., 2012. Pristine Noachian crust and key geologic transitions in the lower walls of Valles

Marineris: Insights into early igneous processes on Mars. Icarus 221, 420–435. http://dx.doi.org/10.1016/j.icarus.2011.12.027.
Fueten, F., Flahaut, J., Le Deit, L., Stesky, R., Hauber, E., Gwinner, K., 2011. Interior layered deposits within a perched basin, southern Coprates Chasma, Mars: Evidence for their formation, alteration, and erosion. J. Geophys. Res. 116. http://dx.doi.org/10.1029/2010JE003695.
Gendrin, A. et al., 2005. Sulfate in martian layered terrains: The OMEGA/Mars Express view. Science 307, 1587–1591.
Grant, J.A., Wilson, S.A., 2011. Late alluvial fan formation in southern Margaritifer Terra, Mars. Geophys. Res. Lett. 38, L08201.
Grant, J.A., Wilson, S.A., 2012. A possible synoptic source of water for alluvial fan formation in southern Margaritifer Terra, Mars. Planet. Space Sci. 72, 44–52. http://dx.doi.org/10.1016/j.pss.2012.05.020.
Grant, J.A. et al., 2011. The science process for selecting the landing site for the 2011 Mars Science Laboratory. Planet. Space Sci. 59, 1114–1127. http://dx.doi.org/10.1016/j.pss.2010.06.016.
Howard, A.D., Moore, J.M., 2011. Late Hesperian to early Amazonian midlatitude martian valleys: Evidence from Newton and Gorgonum basins. J. Geophys. Res. 116, E05003. http://dx.doi.org/10.1029/2010JE003782.
Hynek, B.M., Phillips, R.J., Arvidson, R.E., 2003. Explosive volcanism in the Tharsis region: Global evidence in the martian geologic record. J. Geophys. Res. 108 (E9), 15. http://dx.doi.org/10.1029/2003JE002062.
Jaumann, R. et al., 2007. The high-resolution stereo camera (HRSC) experiment on Mars Express: Instrument aspects and experiment conduct from interplanetary cruise through the nominal mission. Planet. Space Sci. 55, 928–952. http://dx.doi.org/10.1016/j.pss.2006.12.003.
King, P.L., McSween, H.Y., 2005. Effects of H_2O, pH, and oxidation state on the stability of Fe minerals on Mars. J. Geophys. Res. 110. http://dx.doi.org/10.1029/2005JE002482.
Kirk, R.L. et al., 2008. Ultrahigh resolution topographic mapping of Mars with MRO HiRISE stereo images: Meter-scale slopes of candidate Phoenix landing sites. J. Geophys. Res. 113, E00A24. http://dx.doi.org/10.1029/2007JE003000.
Klingelhöfer, G. et al., 2004. Jarosite and hematite at Meridiani Planum from Opportunity's Mössbauer spectrometer. Science 306, 1740–1745. http://dx.doi.org/10.1126/science.1104653.
Komatsu, G., Geissler, P.E., Strom, R.G., Singer, R.B., 1993. Stratigraphy and erosional landforms of layered deposits in Valles Marineris, Mars. J. Geophys. Res. 98 (E6), 11105–11121.
Langevin, Y., Poulet, F., Bibring, J.-P., Gondet, B., 2005. Sulphates in the northern region of Mars detected by OMEGA/Mars Express. Science 307, 1584–1586.
Le Deit, L., Bourgeois, O., Mège, D., Hauber, E., Le Mouélic, S., Massé, M., Jaumann, R., Bibring, J.-P., 2010. Morphology, stratigraphy, and mineralogical composition of a layered formation covering the plateaus around Valles Marineris, Mars: Implications for its geological history. Icarus 208 (2), 684–703.
Liu, Y., Arvidson, R.E., Catalano, J.G., 2013. Spectral identification and stratigraphic study of phyllosilicates and hydrated sulfates in the southwestern of Melas Chasma and environmental implications on Mars. Lunar Planet. Sci. 44. Abstract 1645.
Lucchitta, B.K., 1990. Young volcanic deposits in the Valles Marineris, Mars? Icarus 86, 476–509. http://dx.doi.org/10.1016/0019-1035(90)90230-7.
Lucchitta, B.K., Isbell, N.K., Howington-Kraus, A., 1994. Topography of Valles Marineris: Implications for erosional and structural history. J. Geophys. Res. 99 (E2), 3783–3798.
Madden, M.E.E., Bodnar, R.J., Rimstidt, J.D., 2004. Jarosite as an indicator of water-limited chemical weathering on Mars. Nature 431, 821–823. http://dx.doi.org/10.1038/nature02934.
Madejová, J., Pentrák, M., Pálková, H., Komadel, P., 2009. Near-infrared spectroscopy: A powerful tool in studies of acid-treated clay minerals. Vib. Spectrosc. 49, 211–218.
Malin, M.C., Edgett, K.S., 2000. Sedimentary rocks of early Mars. Science 290, 1927–1937.
Malin, M.C., Edgett, K.S., 2001. Mars Global Surveyor Mars Orbiter Camera: Interplanetary cruise through primary mission. J. Geophys. Res. 106 (E10), 23429–23570.
Malin, M.C. et al., 2007. Context Camera Investigation on board the Mars Reconnaissance Orbiter. J. Geophys. Res. 112, E05S04. http://dx.doi.org/10.1029/2006JE002808).
Mangold, N., Quantin, C., Ansan, V., Delacourt, C., Allemand, P., 2004. Evidence for precipitation on Mars from dendritic valleys in the Valles Marineris area. Science 305, 78–81.
Mangold, N.A. et al., 2008. Spectral and geological study of the sulfate-rich region of West Candor Chasma, Mars. Icarus 194, 519–543. http://dx.doi.org/10.1016/j.icarus.2007.10.021.
Mangold, N., Roach, L., Milliken, R., Le Mouélic, S., Ansan, V., Bibring, J.-P., Masson, P., Mustard, J.F., Murchie, S., Neukum, G., 2010. A Late Amazonian alteration layer related to local volcanism on Mars. Icarus 207, 265–276. http://dx.doi.org/10.1016/j.icarus.2009.10.015.
Masse, M., Bourgeois, O., Le Mouelic, S., Verpoorter, C., Le Deit, L., Bibring, J.P., 2011. Martian polar and circum-polar sulfate-bearing deposits: Sublimation tills derived from the North Polar Cap. Icarus 209, 434–451. http://dx.doi.org/10.1016/j.icarus.2010.04.017.
McCauley, J.F., 1978. Geologic Map of the Coprates Quadrangle of Mars, Scale 1:5,000,000. U.S. Geol. Surv. Misc. Inv. Series Map I-897.
McEwen, A.S. et al., 2007. Mars Reconnaissance Orbiter's High Resolution Imaging Science Experiment (HiRISE). J. Geophys. Res. 112, E05S02. http://dx.doi.org/10.1029/2005JE002605).
Metz, J.M. et al., 2009. Sublacustrine depositional fans in southwest Melas Chasma. J. Geophys. Res. 114 (E10002).
Metz, J., Grotzinger, J., Okubo, C., Milliken, R., 2010. Thin-skinned deformation of sedimentary rocks in Valles Marineris, Mars. J. Geophys. Res. 115. http://dx.doi.org/10.1029/2010JE003593.
Michalski, J.R., Niles, P.B., 2012. Atmospheric origin of martian interior layered deposits: Links to climate change and the global sulfur cycle. Geology. http://dx.doi.org/10.1130/G32971.1.
Milliken, R.E. et al., 2008. Opaline silica in young deposits on Mars. Geology 36, 847–7580. http://dx.doi.org/10.1130/G24967A.1.
Murchie, S. et al., 2007. Compact Reconnaissance Imaging Spectrometer for Mars (CRISM) on Mars Reconnaissance Orbiter (MRO). J. Geophys. Res. 112, E05S03. http://dx.doi.org/10.1029/2006JE002682).
Murchie, S.L. et al., 2009a. Compact Reconnaissance Imaging Spectrometer for Mars investigation and data set from the Mars Reconnaissance Orbiter's primary science phase. J. Geophys. Res. 114, E00D07. http://dx.doi.org/10.1029/2009JE00334.
Murchie, S.L. et al., 2009b. A synthesis of martian aqueous mineralogy after 1 Mars year of observations from the Mars Reconnaissance Orbiter. J. Geophys. Res. 114, E00D06. http://dx.doi.org/10.1029/2009JE003342.
Murchie, S. et al., 2009c. Evidence for the origin of layered deposits in Candor Chasma, Mars, from mineral composition and hydrologic modeling. J. Geophys. Res. 114, E00D05. http://dx.doi.org/10.1029/2009JE003343.
Nedell, S.S., Squyres, S.W., Andersen, D.W., 1987. Origin and evolution of the layered deposits in the Valles Marineris, Mars. Icarus 70, 409–441.
Niles, P.B., Michalski, J., 2009. Meridiani sediments on Mars formed through weathering in massive ice deposits. Nat. Geosci. 2. http://dx.doi.org/10.1038/NGEO438.
Noe Dobrea, E., Michalski, J., Swayze, G., 2011. Aqueous mineralogy and stratigraphy at and around the proposed Mawrth Vallis MSL landing site: New insights into the aqueous history of the region. Mars 6, 32–46. http://dx.doi.org/10.1555/mars.2011.0003.
Noe Dobrea, E.Z., Wray, J.J., Calef III, F.J., Parker, T.J., Murchie, S.L., 2012. Hydrated minerals on Endeavour Crater's rim and interior, and surrounding plains: New insights from CRISM data. Geophys. Res. Lett. 38 (23). http://dx.doi.org/10.1029/2012GL053180.
Pelkey, S.M. et al., 2007. CRISM multispectral summary products: Parameterizing mineral diversity on Mars from reflectance. J. Geophys. Res. 112, E08S14. http://dx.doi.org/10.1029/2006JE002831.
Peterson, C., 1982. A secondary origin for the central plateau of Hebes Chasma. In: Merrill, R.B., Ridings, R. (Eds.), Proceedings of the 12th Lunar and Planetary Science Conference. Pergamon Press, New York and Oxford, pp. 1459–1471.
Prothero, D.R., Schwab, F., 2004. Sedimentary Geology. An Introduction to Sedimentary Rocks and Stratigraphy, second ed. W.H. Freeman and Co., New York.
Quantin, C., Allemand, P., Mangold, N., Dromart, G., Delacourt, C., 2005. Fluvial and lacustrine activity on layered deposits in Melas Chasma, Valles Marineris, Mars. J. Geophys. Res. 110. http://dx.doi.org/10.1029/2005JE002440.
Roach, L.H. et al., 2009. Testing evidence of recent hydration state change in sulfates on Mars. J. Geophys. Res. 114, E00D02. http://dx.doi.org/10.1029/2008JE003245.
Roach, L.H., Mustard, J.F., Swayze, G., Milliken, R.E., Bishop, J.L., Ehlmann, B.L., Murchie, S.L., Lichtenberg, K., 2010. Hydrated mineral stratigraphy of Ius Chasma, Valles Marineris. Icarus 206, 253–268.
Robertson, K., Bish, D., 2013. Constraints on the distribution of $CaSO_4nH_2O$ phases on Mars and implications for their contribution to the hydrological cycle. Icarus 223, 407–417. http://dx.doi.org/10.1016/j.icarus.2012.10.028.
Rossi, A.P. et al., 2008. Large-scale spring deposits on Mars? J. Geophys. Res. 113, E08016. http://dx.doi.org/10.1029/2007JE003062.
Schultz, R.A., 1998. Multiple-process origin of Valles Marineris basins and troughs, Mars. Planet. Space Sci. 46, 827–829. http://dx.doi.org/10.1016/ S0032-0633(98)00030-0.
Scott, D.H., Tanaka, K.L., 1986. Geologic Map of the Western Equatorial Region of Mars. U.S. Geol. Surv. Misc. Invest. Ser. Map, I-1802-A.
Seelos, F.P., 2011. CRISM data processing and analysis products update – Calibration, 1076 correction, and visualization. Lunar Planet. Sci. 42. Abstract #1438.
Settle, M., 1979. Formation and deposition of volcanic sulfate aerosols on Mars. J. Geophys. Res. 84. http://dx.doi.org/10.1029/0JGREA000084000B14008343000001.
Spencer, R.J., 2000. Sulfate minerals in evaporite deposits. In: Alpers, C.N., Jambor, J.L., Nordstrom, D.K. (Eds.), Sulfate Minerals: Crystallography, Geochemistry, and Environmental Significance, Rev. Mineral. Geochem., vol. 40. Mineral. Soc. of Am., Washington, DC, pp. 173–192.
Squyres, S.W. et al., 2006. Rocks of the Columbia Hills. J. Geophys. Res. 111, E02S11. http://dx.doi.org/10.1029/2005JE002562.
Squyres, S.W. et al., 2004. The Opportunity rover's Athena Science investigation at Meridiani Planum, Mars. Science 306, 1698–1703. http://dx.doi.org/10.1126/science.1106171.
Squyres, S.W., and the Athena Science Team, 2012. Initial Opportunity rover results at Endeavour Crater, Mars. Lunar Planet. Sci. 43. Abstract 1892.
Stoffregen, R.E., Alpers, C.N., Jambor, J.L., 2000. Alunite–jarosite crystallography, thermodynamics, and geochemistry. In: Alpers, C.N., Jambor, J.L., Nordstrom, D.K. (Eds.), Sulfate Minerals: Crystallography, Geochemistry, and Environmental Significance, Reviews in Mineralogy, vol. 40. Mineral. Soc. Am., Washington, DC, pp. 453–479.

Please cite this article in press as: Weitz, C.M., et al. Mixtures of clays and sulfates within deposits in western Melas Chasma, Mars. Icarus (2014), http://dx.doi.org/10.1016/j.icarus.2014.04.009

Thollot, P. et al., 2012. Most Mars minerals in a nutshell: Various alteration phases formed in a single environment in Noctis Labyrinthus. J. Geophys. Res. 117, E00J06. http://dx.doi.org/10.1029/2011JE004028.

Tosca, N.J., Milliken, R.E., Wyatt, M.B., McLennan, S.M., 2008a. Clay minerals and poorly crystalline silicates: Unravelling paleo-acidity at the martian surface. Lunar Planet. Sci. XXXIX. Abstract 1745.

Tosca, N.J., Knoll, A.H., McLennan, S.M., 2008b. Water activity and the challenge for life on early Mars. Science 320, 1204–1207.

Van Driessche, A.E.S., Benning, L.G., Rodriguez-Blanco, J.D., Ossorio, M., Bots, P., Garcia-Ruiz, J.M., 2012. The role and implications of bassanite as a stable precursor phase to gypsum precipitation. Science 336. http://dx.doi.org/10.1126/science.1215648.

Vaniman, D.T., Chipera, S.J., 2006. Transformations of Mg- and Ca-sulfate hydrates in Mars regolith. Am. Mineral. 91, 1628–1642. http://dx.doi.org/10.2138/am.2006.2092.

Vaniman, D.T., Chipera, S.J., Carey, J.W., 2006. Hydration experiments and physical observations at 193 K and 243 K for Mg-sulfates relevant to Mars. Lunar Planet. Sci. XXXVII. Abstract 144.

Vaniman, D.T., Bish, D.L., Chipera, S.J., 2008. Calcium sulfate hydration, stability and transformation on Mars. Lunar Planet. Sci. XXXIX. Abstract 1816.

Vaniman, D.T. et al., 2013. Mineralogy of a mudstone at Yellowknife Bay, Gale Crater, Mars. Science. http://dx.doi.org/10.1126/science.1243480.

Weitz, C.M., Parker, T.J., Bulmer, M.H., Anderson, F.S., Grant, J.A., 2003. Geology of the Melas Chasma landing site for the Mars Exploration Rover mission. J. Geophys. Res. 108 (E12), 8082. http://dx.doi.org/10.1029/2002JE002022.

Weitz, C.M., Milliken, R.E., Grant, J.A., McEwen, A.S., Williams, R.M.E., Bishop, J.L., Thompson, B.J., 2010. Mars Reconnaissance Orbiter observations of light-toned layered deposits and associated fluvial landforms on the plateaus adjacent to Valles Marineris. Icarus 205 (1), 73–102. http://dx.doi.org/10.1016/j.icarus.2009.04.017.

Weitz, C.M., Bishop, J.L., Thollot, P., Mangold, N., Roach, L.H., 2011. Diverse mineralogy in two troughs of Noctis Labyrinthus, Mars. Geology 39, 899–902. http://dx.doi.org/10.1130/G32045.1.

Weitz, C.M., Noe Dobrea, E.Z., Lane, M.D., Knudson, A., 2012. Geologic relationships between gray hematite, sulfates, and clays in Capri Chasma. J. Geophys. Res. 117, E00J09. http://dx.doi.org/10.1029/2012JE004092.

Weitz, C.M., Noe Dobrea, E., Wray, J.J., 2013a. Gypsum, jarosite, and other minerals associated with a blocky deposit in western Melas Chasma. Lunar Planet. Sci. XXXXIV. Abstract 2076.

Weitz, C.M., Bishop, J.L., Grant, J.A., 2013b. Gypsum, opal, and fluvial channels within a trough of Noctis Labyrinthus, Mars: Implications for aqueous activity during the Late Hesperian to Amazonian. Planet. Space Sci. 87, 130–145. http://dx.doi.org/10.1016/j.pss.2013.08.007.

Williams, R.E., and Weitz, C.M. (2014), Reconstructing the aqueous history within the southwestern Melas Basin: Clues from stratigraphic and morphometric analyses of fans, Icarus, Submitted for publication.

Wray, J.J., Squyres, S.W., Roach, L.H., Bishop, J.L., Mustard, J.F., Noe Dobrea, E.Z., 2010. Identification of the Ca-sulfate bassanite in Mawrth Vallis, Mars. Icarus 209, 416–421. http://dx.doi.org/10.1016/j.icarus.2010.06.001.

Wray, J.J. et al., 2011. Columbus crater and other possible groundwaterfed paleolakes of Terra Sirenum, Mars. J. Geophys. Res. 116, E01001. http://dx.doi.org/10.1029/2010JE003694.

Yen, A.S. et al., 2008. Hydrothermal processes at Gusev Crater: An evaluation of Paso Robles class soils. J. Geophys. Res. 113, E06S10. http://dx.doi.org/10.1029/2007JE002978.

Zuber, M.T. et al., 1992. The Mars Observer Laser Altimeter investigation. J. Geophys. Res. 97, 7781–7797.

Please cite this article in press as: Weitz, C.M., et al. Mixtures of clays and sulfates within deposits in western Melas Chasma, Mars. Icarus (2014), http://dx.doi.org/10.1016/j.icarus.2014.04.009